This paper appears in IEEE Control Systems Magazine, 2017.
DOI: 10.1109/MCS.2017.2696760

Nonlinear disturbance observers

Design and applications to Euler-Lagrange systems

Alireza Mohammadi, Horacio J. Marquez, and Mahdi Tavakoli
POC: H. J. Marquez (hmarquez@ualberta.ca)

August 26, 2016

Estimation of unknown inputs and/or disturbances has been a topic of constant interest in the control engineering for the past several decades. The reader is referred to [1] for a detailed survey on the development of unknown input observers. Disturbance observers (DOB) are a special class of unknown input observers that were introduced for robust motion control applications in the early 1980s [2]. Since their introduction in the literature, DOBs have been employed efficaciously in numerous robust control and fault detection applications ranging from process control [3], [4] to mechatronics [5], [6], [7], [8], [9]. Figure 1 depicts a DOB that is employed in a typical control system. As can be seen in the figure, the DOB is used to reconstruct unknown disturbances that are acting on the plant from the measured output variables and the known control inputs applied to the system. The output of the DOB, namely, the estimated disturbance, can then be used in feedforward compensation of disturbances or faults.

Disturbance observers possess several promising features in control applications [10]. The most important feature is the add-on or "patch" feature. The disturbance feedforward compensation can be employed as an add-on to a previously designed feedback control. Indeed, there is no need to change the existing control laws, which might have been extensively used and established in their respective literatures, such as PID feedback control used in industrial systems, model predictive control used in process systems, and gain scheduling feedback control used in flight control. In order to improve the disturbance rejection and robustness abilities, DOB-based compensation can be augmented with the baseline feedback control designed using conventional techniques. This feature has made using DOBs an appealing approach for rejecting disturbances in commercial control applications. See [11] for a discussion on commercialization aspects of DOBs.

In general, DOB design has been carried out using linear system techniques [12], [13], [5], [14], [15], [16], [17], [18], [19]. In order to overcome the limitations of linear disturbance observers (LDOB) in the presence of highly nonlinear and coupled dynamics, researchers have started investigating nonlinear disturbance observers (NDOB) for systems with nonlinear

TABLE 1: An overview of nonlinear disturbance observer (NDOB) classes: Based on their underlying dynamical equations and similarity to state observers, NDOBs can be categorized into two classes; namely, basic NDOBs and sliding mode-based NDOBs.

NDOB class	References	Applications
Basic	[20], [27], [28] [29], [30], [31]	mechatronics, robotics, and teleoperation
Sliding mode-like	[32], [33], [34] [35], [36]	robust fault detection, attitude and formation control in aerospace applications

dynamics during the past decade [20], [21], [22], [23], [24]. A line of research has also been initiated to address some of the more theoretical questions that arise in the context of NDOBs [23], [25], [26] where singular perturbation and time-scale separation analyses have been employed. The papers [23], [25], [26] have also extensively studied the problem of recovering nominal transient performance in the presence of disturbances using NDOBs. There exist various types of NDOBs proposed in the literature and each of them is suitable for a specific set of applications. A possible way to categorize NDOBs is to consider their underlying dynamical equations to state observers. Based on this criterion, NDOBs can be categorized into two general classes; namely, basic NDOBs and sliding mode-based NDOBs. Basic NDOBs are extensively used in mechatronics and robotics applications and are the generalization of the famous linear DOB in [12], [5] to the context of systems with nonlinear dynamics. Sliding mode-like NDOBs are appealing in applications where disturbance estimation error needs to converge in finite time such as fault-detection applications. Presence of discontinuities in the sliding mode-based NDOBs, which may give rise to the chattering phenomenon, make their analysis harder. Table 1 gives an overview of the existing NDOBs and their applications.

One of the restrictions of disturbance observers is that they require measurement of the states of the dynamical control system under study. A relatively new research direction in the DOB framework is to combine state and disturbance observers in the so-called generalized extended state observer framework which is essentially an output-based disturbance observer (see [37], [38] for further details).

One of the most prominent applications of NDOBs is in the field of robotics. Various types of disturbances such as joint frictions, unknown payloads, and varying contact points might adversely affect the stability and performance of the robotic control systems. By exploiting the special structure of dynamical equations of robotic systems, NDOB design takes a special form. A general NDOB gain design method for serial robotic manipulators, which builds upon the

work in [39], [21], has been recently proposed in the literature [29], [40]. The proposed NDOB gain can accommodate conventional LDOB/NDOB gains that were previously proposed in the literature [5], [39] and remove the previously existing restrictions on the types of joints, the manipulator configuration, or the number of degrees-of-freedom (DOFs). Since its introduction, this design method has been applied to other class of robotic systems such as observer-based control of 6-DOF parallel manipulators [30], improving transparency in virtual coupling for haptic interaction during contact tasks [31], and dynamic surface control of mobile wheeled inverted pendulums [41]. This serves as the motivation to investigate whether the NDOB structure in [29] can be applied to the more general class of Euler-Lagrange (EL) systems. Euler-Lagrange models can be effectively used to describe a plethora of physical systems ranging from mechanical and electromechanical to power electronic and power network systems [42], [43], [44], [45]. In this article, the focus of applications is on robotic systems possessing EL dynamics.

One of the latest applications of DOBs has been in the field of teleoperation where there is a need for stability and transparency [46], [47], [48], [49], [16], [50]. Teleoperation involves indirect performance of a task in a remote environment and is used to extend a person's sensing and manipulation capability to a remote location [51]. Every teleoperation system consists of a master robot (user interface) and a slave robot, which exchange different types of information such as force, position, and visual and auditory data via a communication channel (see Figure 2). The master interacts with the human operator and the slave interacts with the remote environment. The human operator applies position commands to the master robot. The slave robot responds to the received position commands from the communication channel and moves to the desired position in the remote environment. If force feedback from the slave side to the master side is present, the system is called a *bilateral teleoperation system* to distinguish it from a *unilateral teleoperation system*, in which no force is reflected to the user. A bilateral teleoperation system is said to be *transparent* if the slave robot follows the position of the master robot and the master robot faithfully displays the slave-environment contact force to the human operator. Major challenges encountered in control of teleoperation systems include nonlinearities and uncertainties, communication delays, and unknown disturbances.

Uncertainties, nonlinearities, and possible time delays in the communication channel constitute the "must solve" problem, given that they can compromise system stability, which must be guaranteed at any cost. A secondary problem, which is also of critical importance, is disturbance rejection. Indeed, rejecting the effect of unknown disturbances is critical given that robust performance and stability largely depends on being able to do so. A promising approach to suppressing such disturbances is to make use of NDOBs.

In this article, NDOB design and its applications to Euler-Lagrange and teleoperation

systems are presented. First, the earliest variant of LDOBs, proposed in [2] (see also [12]) and which has inspired the research on DOBs, is briefly described to motivate further the development of its nonlinear counterpart. Next, the structure of an NDOB proposed in [21] (see also [10], [11]), that has a basic structure and can be effectively employed in EL and teleoperation systems, is presented. Some properties of this class of NDOBs such as semi/quasi-passivity property, which have not been discussed in the previous NDOB literature, are presented in this article.

We then turn to EL systems and present the general observer design method, which is based on the NDOB structure in [39], [21], for this class of dynamical systems. We show that the NDOB structure in [29], which was first proposed for serial robotic manipulators, can be used for the more general class of EL systems. Moreover, we show how the proposed NDOB can be used along with well-established control schemes such as passivity-based control.

As an important application, NDOBs are incorporated into the framework of the 4-channel teleoperation architecture. This control architecture is used extensively to achieve full transparency in the *absence of time delays* [52], [53], [54]. Unfortunately, it is well known that unless disturbances are explicitly accounted for during the design, their presence may cause poor position/force tracking or even instability of the 4-channel teleoperation system. The proposed NDOB enables the 4-channel teleoperation architecture to achieve full transparency and exponential disturbance and position tracking under slow-varying disturbances. In the case of fast-varying disturbances, the proposed NDOBs guarantee global uniform ultimate boundedness of the tracking errors. In this article, it is demonstrated how the proposed NDOB can be accommodated in the 4-channel bilateral teleoperation architecture to guarantee stability and transparency of the teleoperation system in the presence of disturbances and in the absence of communication delays.

Throughout the rest of the article we will employ the following notation:

Notation. We let $\mathbb{R}$, $\mathbb{R}^+$, and $\mathbb{R}_0^+$ denote the field of real numbers, and the sets of positive and nonnegative real numbers, respectively. $\mathbb{R}^n$ represents the set of n-dimensional vectors with real components. The maximum and the minimum eigenvalues of a square matrix are represented by $\lambda_{\max}(.)$ and $\lambda_{\min}(.)$, respectively. Euclidean norm and induced matrix 2-norm are used to define vector and matrix norms. In other words, $|x| = \sqrt{x^T x}$ represents the vector norm for a given vector $x \in \mathbb{R}^n$. Likewise, $\left|X\right| = \sqrt{\lambda_{\max}(X^T X)}$ for a given matrix $X \in \mathbb{R}^{n\times n}$. Given two square matrices A, $B \in \mathbb{R}^{n\times n}$, the inequality $A \geq B$ means that $A - B$ is a positive semi-definite matrix.

Linear Disturbance Observer

Since the focus of this article is on NDOBs, only the first variant of LDOBs will be briefly presented. This DOB was first proposed in [2], [12] for robust motion control systems and has since motivated much research in the control community. Rigorous analyses and definitions will be presented in the context of NDOBs in the next section. For a detailed discussion on other variants of LDOBs, the reader is referred to [1], [10], [55], [11] and references therein.

Figure 3 demonstrates the block diagram of a DOB-based robust motion control system proposed in [2], [12]. The torque τ represents the control input is represented. Moreover, the parameters J and $L_{\rm d}$ represent mass/inertia and gain of the DOB, which is a design parameter, respectively. The unknown disturbance $\tau_{\rm d}$ lumps the effect of disturbances such as harmonics and friction; namely,

$$\tau_{\rm d} = \tau_{\rm d,f} + \tau_{\rm d,h},$$

where $\tau_{\rm d,f}$ and $\tau_{\rm d,h}$ are the friction and harmonic disturbances, respectively. Similarly, other disturbances can be incorporated in the lumped disturbance $\tau_{\rm d}$.

The role of the DOB in Figure 3 is to estimate the lumped disturbance torque $\tau_{\rm d}$ from the state $\dot{\theta}$ and input torque τ. The equation of motion is given by

$$J\ddot{\theta} = \tau + \tau_{\rm d} - \hat{\tau}_{\rm d}.$$

Feeding forward the disturbance estimate $\hat{\tau}_{\rm d}$ suppresses the adverse effect of $\tau_{\rm d}$ on the motion control system in Figure 3. In the ideal case, when $\hat{\tau}_{\rm d} = \tau_{\rm d}$, the lumped disturbance will be canceled out and the control input τ acts on the nominal control system with no disturbances. As it can be seen from the block diagram in Figure 3

$$\hat{\tau}_{\rm d} = -\frac{L_{\rm d}}{s + L_{\rm d}}\big(JL_{\rm d}\dot{\theta} + \tau - \hat{\tau}_{\rm d}\big) + JL_{\rm d}\dot{\theta} = \frac{L_{\rm d}}{s + L_{\rm d}}(Js\dot{\theta} + \tau - \hat{\tau}_{\rm d}).$$

Therefore, the disturbance estimate satisfies

$$\hat{\tau}_{\rm d} = \frac{L_{\rm d}}{s + L_{\rm d}}\tau_{\rm d} = \frac{1}{\frac{1}{L_{\rm d}}s + 1}\tau_{\rm d}.$$

If the lumped disturbance term $\tau_{\rm d}$ remains within the bandwidth of the DOB, it can be accurately estimated by the output of the DOB, namely, $\hat{\tau}_{\rm d}$. Indeed, larger DOB gains give rise to better transient responses in estimation. The nonlinear counterpart of this property of DOBs is shown in the next sections.

Nonlinear Disturbance Observer

In this section, the general NDOB structure of [21] and some of its properties that have not been discussed in the previous NDOB literature are presented. In particular, semi/quasi-passivity and uniform ultimate boundedness (see "Brief Review of Nonlinear Systems" for the definition of these two concepts) of this class of NDOBs are discussed in this section. The NDOB gain design for EL systems will be presented in the next section.

Nonlinear disturbance observer structure and assumptions on disturbances

Consider the following nonlinear control affine system

$$\begin{aligned} \dot{x} &= f(x) + g_1(x)u + g_2(x)d, \\ y &= h(x), \end{aligned} \tag{1}$$

where $x \in \mathbb{R}^n$ is the state vector, $u \in \mathbb{R}^m$ is the control input vector, $d \in \mathbb{R}^l$ is the lumped disturbance vector, and $y \in \mathbb{R}^m$ is the output vector. The lumped disturbance vector d is assumed to lump the effect of unknown disturbances. The functions f, g_1, and g_2 in (1) are assumed to be smooth. Additionally, the functions f and g_1 represent the nominal model of the system.

The problem to solve is to design an observer, called the disturbance observer, to estimate the lumped disturbance vector d from the state and input vectors. The output of the DOB can be used in feedforward compensation of disturbances.

An NDOB structure, proposed in [21] (see also [10], [11]), that can be employed to estimate the lumped disturbance vector d is

$$\begin{aligned} \dot{z} &= -L_{\rm d}(x)g_2(x)z - L_{\rm d}(x)\big[f(x) + g_1(x)u + g_2(x)p(x)\big], \\ \hat{d} &= z + p(x), \end{aligned} \tag{2}$$

where $z \in \mathbb{R}^l$ is the internal state vector of the DOB, $\hat{d} \in \mathbb{R}^l$ is the estimated disturbance

vector, and $p(x)$ is called the auxiliary vector of the NDOB. Finally, the matrix $L_{\rm d}(x)$ is called the NDOB gain matrix. As it will be shown in this section, there should exist a certain relation between the auxiliary vector $p(x)$ and the NDOB gain $L_{\rm d}(x)$. Figure 4 depicts the block diagram of the NDOB-based robust control system proposed in [21]. The disturbance tracking error is defined to be

$$e_{\rm d} := \hat{d} - d. \tag{3}$$

Before presenting the disturbance tracking error dynamics of the NDOB (2), we provide a brief sketch of how this NDOB is derived. Taking the derivative of (3) and assuming $\dot{d} \approx 0$ yields

$$\dot{e}_{\rm d} = \dot{\hat{d}}.$$

We would like the estimation error to asymptotically converge to zero. Therefore, it is desirable to have

$$\dot{e}_{\rm d} = \dot{\hat{d}} = -Le_{\rm d},$$

where $L = \alpha_{\rm d} I$ and $\alpha_{\rm d}$ is some positive scalar. By (3), we have

$$\dot{\hat{d}} = -L\big(\hat{d} - d\big).$$

Assuming that $g_2(x) \in \mathbb{R}^{n\times l}$ has full column rank for all x, we define the following gain matrix

$$L_{\rm d}(x) := \alpha_{\rm d} g_2^{\dagger}(x), \tag{4}$$

where $g_2^{\dagger}(x)$ is a left inverse of $g_2(x)$, e.g., $g_2^{\dagger}(x) = \big(g_2^T(x)g_2(x)\big)^{-1} g_2^T(x)$. Then, $L_{\rm d}(x)g_2(x) = L$. Hence, from (1), we have

$$\dot{\hat{d}} = -L\big(\hat{d} - d\big) = -L_{\rm d}(x)g_2(x)\hat{d} + \underbrace{L_{\rm d}(x)g_2(x)d}_{L_{\rm d}(x)\left(\dot{x} - f(x) - g_1(x)u\right)}.$$

Accordingly,

$$\dot{\hat{d}} = -L_{\rm d}(x)g_2(x)\hat{d} + L_{\rm d}(x)\dot{x} - L_{\rm d}(x)\big(f(x) + g_1(x)u\big).$$

Before proceeding further, we remark that if the derivative of the state x is assumed to be available, then design is completed at this stage. This is the case for the 4-channel control architecture used in teleoperation systems where there are accelerometers available. This is further discussed later in the article. Defining the variable $z := \hat{d} - p(x)$ and inserting in the above equation, we get

$$\dot{z} + \dot{p}(x) = -L_{\rm d}(x)g_2(x)z + L_{\rm d}(x)g_2(x)p(x) + L_{\rm d}(x)\dot{x} - L_{\rm d}(x)\big(f(x) + g_1(x)u\big).$$

Therefore, if the relation

$$L_{\mathrm{d}}(x) = \frac{\partial p}{\partial x}(x), \tag{5}$$

holds between the NDOB gain matrix $L_{\mathrm{d}}(x)$ and the auxiliary vector $p(x)$, then

$$\dot{p}(x) = L_{\mathrm{d}}(x)\dot{x},$$

and we get the given expression for the NDOB given by (2).

Taking the derivative of (3), the tracking error dynamics can be computed as follows

$$\begin{aligned}
\dot{e}_{\mathrm{d}} &= \dot{\hat{d}} - \dot{d} \underbrace{=}_{(2)} \dot{z} + \dot{p}(x) - \dot{d} = -L_{\mathrm{d}}(x)g_2(x)z - L_{\mathrm{d}}(x)\big[\underbrace{f(x) + g_1(x)u}_{\dot{x} - g_2(x)d} + g_2(x)p(x)\big] + \dot{p}(x) - \dot{d} \\
&= -L_{\mathrm{d}}(x)g_2(x)z - L_{\mathrm{d}}(x)\big[\dot{x} + g_2(x)(\underbrace{p(x)}_{\hat{d}-z} - d)\big] + \dot{p}(x) - \dot{d} \\
&= -L_{\mathrm{d}}(x)g_2(x)z - L_{\mathrm{d}}(x)\big[\dot{x} + g_2(x)e_{\mathrm{d}} - g_2(x)z\big] + \dot{p}(x) - \dot{d} \\
&= -L_{\mathrm{d}}(x)g_2(x)e_{\mathrm{d}} - L_{\mathrm{d}}(x)\dot{x} + \dot{p}(x) - \dot{d}.
\end{aligned}$$

Using (5) in the above expression, it can be seen that the disturbance tracking error dynamics are governed by

$$\dot{e}_{\mathrm{d}} = -L_{\mathrm{d}}(x)g_2(x)e_{\mathrm{d}} - \dot{d}. \tag{6}$$

It is assumed that the observer gain $L_{\mathrm{d}}(x)$ has been designed to satisfy

$$-e_{\mathrm{d}}^T L_{\mathrm{d}}(x)g_2(x)e_{\mathrm{d}} \leq -\alpha_{\mathrm{d}}|e_{\mathrm{d}}|^2, \tag{7}$$

uniformly with respect to x for some positive constant α_{d}. In general, design of the NDOB gain matrix $L_{\mathrm{d}}(x)$ is not trivial. As it can be seen from Equation (7), one needs to know the structure of $g_2(x)$ in order to design the gain matrix $L_{\mathrm{d}}(x)$. Therefore, determining this gain depends on the application under study. In the case of Euler-Lagrange systems and due to the special structure of the underlying dynamical equations, we are able to find such a gain matrix. Under the assumption that $g_2(x)$ has full row rank for all x, which is also the case for Euler-Lagrange systems under study in this article, an expression for $L_{\mathrm{d}}(x)$ is given in (**??**). The issue of designing $L_{\mathrm{d}}(x)$ for EL systems will be discussed in the next section. In order to analyze how

the NDOB in (2) achieves disturbance tracking, the Lyapunov candidate function $V_{\mathrm{d}} = \frac{1}{2} e_{\mathrm{d}}^T e_{\mathrm{d}}$ is considered. Taking the derivative of V_{d} along the trajectories of (6) yields

$$\dot{V}_{\mathrm{d}} = -e_{\mathrm{d}}^T L_{\mathrm{d}}(x) g_2(x) e_{\mathrm{d}} - e_{\mathrm{d}}^T \dot{d}. \tag{8}$$

Some prior knowledge regarding the lumped disturbance dynamics is required in order to analyze further the performance of an NDOB in terms of stability and disturbance tracking. In this article, it is assumed that there exists a positive real constant ω such that

$$|\dot{d}(t)| \leq \omega, \text{ for all } t \geq 0. \tag{9}$$

We remark that the constant ω needs not be known precisely. The NDOB stability analysis only requires knowing some upper bounds on ω. The interested reader is referred to [19], [11] for a detailed discussion on estimating higher order disturbances in time series expansion, and to [21] in the case that the disturbances are generated by linear exosystems with known dynamics. Note also that assumption (9) does not require knowing any special form for the lumped disturbance. Indeed, the ability to estimate unknown disturbances without the need for knowing their special form has been one of the key motivations behind DOB research [5].

Finally, we assume that the disturbance d satisfies the *matching condition*; namely, there exists a smooth function $g_{\mathrm{d}}(x)$ such that

$$g_1(x) g_{\mathrm{d}}(x) = g_2(x), \tag{10}$$

where $|g_{\mathrm{d}}(x)| \leq \bar{g}_{\mathrm{d}}$ holds uniformly with respect to x for some positive constant $\bar{g}_{\mathrm{d}}$. In other words, the lumped disturbance d and the control input u act on the system through the same channel. This matching condition serves the application purpose of this article. The interested reader is referred to [24], [38] where progress has been made in order to relax this condition by using tools from geometric nonlinear control. Finally, we assume that $|g_2(x)| \leq \bar{g}_2$ holds uniformly with respect to x for some positive constant $\bar{g}_2$.

In order to investigate the add-on feature of NDOBs, the following DOB-based control input is considered

$$u = u_{\rm n} - \beta_{\rm d} y - g_{\rm d}(x)\hat{d}, \tag{11}$$

where $\beta_{\rm d}$ is some non-negative constant, y is the vector of outputs, $\hat{d}$ is the estimated disturbance provided by the NDOB in (2), and the nominal control input $u_{\rm n}$ is designed for the system without disturbances, namely, the nominal control system

$$\begin{aligned} \dot{x} &= f(x) + g_1(x)u, \\ y &= h(x). \end{aligned} \tag{12}$$

The role of the feedforward term $-g_{\rm d}(x)\hat{d}$ in (11) is to suppress the adverse effects of unknown disturbances acting on the closed-loop system. The nominal closed-loop system vector field is denoted by

$$f^{\rm cl}(x) = f(x) + g_1(x)u_{\rm n}. \tag{13}$$

Under the matching condition and using the DOB-based control input (11) in (1), it can be seen that

$$\begin{aligned} \dot{x} &= f(x) + g_1(x)\big(u_{\rm n} - g_{\rm d}(x)e_{\rm d} - \beta_{\rm d} y\big), \\ y &= h(x). \end{aligned} \tag{14}$$

Semi/Quasi-passivity of NDOBs

In this section, we show that under the assumption of passivity (see "Brief Review of Nonlinear Systems" for the definition of passivity) of the nominal nonlinear system (12), the NDOB (2) is able to make the augmented nonlinear system and the NDOB semi/quasi-passive. This observation regarding the semi/quasi-passivity of the NDOB in [21] has not been reported in the previous NDOB literature. Using (7) and (8) along with (9), it can be seen that

$$\dot{V}_{\rm d} \leq -\alpha_{\rm d}|e_{\rm d}|^2 + \omega|e_{\rm d}|. \tag{15}$$

The first thing to notice in Inequality (15) is that it immediately follows from the uniform ultimate boundedness theorem (see "Brief Review of Nonlinear Systems") that for all $e_{\rm d}(0) \in \mathbb{R}^l$, the disturbance tracking error converges with an exponential rate, proportional to $\alpha_{\rm d}$, to a ball centered at the origin with a radius proportional to $\frac{1}{\alpha_{\rm d}}$. Since the ultimate bound and convergence rate of the NDOB (2) can be changed by tuning the design parameter $\alpha_{\rm d}$, it is said to be *practically stable*. Indeed, increasing the parameter $\alpha_{\rm d}$ results in better disturbance tracking response; that is, both convergence rate and accuracy of the disturbance observer are improved when $\alpha_{\rm d}$ is increased. Note also that when the disturbance is generated by an exogenous system and Inequality (7) holds uniformly with respect to x, the uniform ultimate boundedness of NDOB (2) holds irrespective of the closed-loop dynamics of the nonlinear system (1). It is noteworthy that the NDOB error dynamics, under the assumption of bounded disturbances, are bounded-input bounded-output (BIBO) stable (the reader is referred to [56] for further details). Finally, it is remarked that when $\omega = 0$ the disturbance tracking error $e_{\rm d}$ will converge to zero asymptotically with an exponential rate.

In order to analyze the semi/quasi-passivity property of the nonlinear system (1) along with (2) in the presence of disturbances, the candidate Lyapunov function $V(x, e_{\rm d}) = V_{\rm n}(x) + V_{\rm d}(e_{\rm d})$ is considered, where $V_{\rm n}$ is the candidate Lyapunov function for the nominal control system $\dot{x} = f(x) + g_1(x)u$, with output $y = h(x)$, for which the inequality $\dot{V}_{\rm n}(x, u) \leq y^T u$ holds. Taking the derivative of V and using (14) along with Inequality (15) yields

$$\dot{V} = \dot{V}_{\rm n} + \dot{V}_{\rm d} \leq y^T \big(u_{\rm n} - g_{\rm d}(x) e_{\rm d} - \beta_{\rm d} y\big) - \alpha_{\rm d} |e_{\rm d}|^2 + \omega |e_{\rm d}|. \tag{16}$$

In order to proceed further, Young's Inequality is used; whereby, $a^T b \leq \frac{|a|^2}{2\epsilon} + \frac{\epsilon |b|^2}{2}$ for all vectors $a, b \in \mathbb{R}^N$ and any arbitrary positive constant ϵ. It can be seen that

$$\dot{V} \leq y^T u_{\rm n} - \big(\beta_{\rm d} - \frac{\epsilon}{2}\big)|y|^2 - \underbrace{\big[(\alpha_{\rm d} - \frac{\omega + \bar{g}_{\rm d}}{2\epsilon})|e_{\rm d}|^2 - \frac{\omega\epsilon}{2}\big]}_{H(e_{\rm d})}, \tag{17}$$

for some positive constant ϵ. Therefore, when

$$\begin{aligned} \beta_{\rm d} &\geq \frac{\epsilon}{2}, \\ \alpha_{\rm d} &\geq \frac{\omega + \bar{g}_{\rm d}}{2\epsilon}, \end{aligned} \tag{18}$$

the augmented nonlinear system (1) with NDOB (2) is a semi/quasi-passive system (see "Brief Review of Nonlinear Systems") with input $\tau_{\rm n}$, output y, and $H(e_{\rm d}) = (\alpha_{\rm d} - \frac{\omega+\bar{g}_{\rm d}}{2\epsilon})|e_{\rm d}|^2 - \frac{\omega\epsilon}{2}$. In a similar way, it can also be shown that if the nonlinear system (1) is semi/quasi-passive, the augmented nonlinear system with the NDOB (2) is semi/quasi-passive.

Semi/quasi-passive systems have several appealing properties (see "Brief Review of Nonlinear Systems"). For instance, it can be shown that an output feedback of the form $u_{\rm n} = \xi(y)$ such that $y^T\xi(y) \leq 0$ makes the solutions of the semi-passive system ultimately bounded. It is to be remarked that the semi/quasi-passivity of the augmented nonlinear system (1) with NDOB (2) is a direct result of feeding forward the disturbance estimate provided by the disturbance observer.

According to the inequalities in (18), the damping injection coefficient $\beta_{\rm d}$, can be chosen to be as small as desired, namely, by choosing the constant ϵ to be arbitrarily small, provided that the coefficient $\alpha_{\rm d}$, namely, the convergence rate of disturbance tracking error, is chosen to be sufficiently large. However, there exists a trade-off between the NDOB gain and noise amplification. The reader is referred to [11], [29] for a discussion of choosing an optimal NDOB gain when measurement noise is present.

In this section, the add-on feature of NDOB (2) in companion with exponentially stabilizing nominal control laws is investigated. One of the applications of the presented material in this section is in robotic systems that are controlled by computed-torque/feedback linearizing control laws (see the Section "Properties of augmented EL systems with NDOBs controlled by computed-torque/feedback linearizing schemes"). We assume that the control input $u_{\rm n} = u_{\rm n}(x,t)$ makes the origin of the nominal closed-loop system globally exponentially stable and $f(0) = 0$.

When the control input $u_{\rm n}(x,t)$ makes the origin of the nominal closed-loop system $\dot{x} = f^{\rm cl}(x,t)$, where $f^{\rm cl}(x,t) = f(x) + g_1(x)u_{\rm n}(x,t)$, globally exponentially stable and $f(0) = 0$, according to the converse Lyapunov function theorem (see "Brief Review of Nonlinear Systems"), there exists a function $V_{\rm n}(x,t)$ that satisfies

$$
\begin{aligned}
&c_1|x|^2 \leq V_{\rm n}(x,t) \leq c_2|x|^2,\\
&\frac{\partial V_{\rm n}}{\partial x} f^{\rm cl}(x,t) + \frac{\partial V_{\rm n}}{\partial t} \leq -c_3|x|^2,\\
&\left|\frac{\partial V_{\rm n}}{\partial x}\right| \leq c_4|x|,
\end{aligned}
\tag{19}
$$

for some positive constants c_1, c_2, c_3, and c_4. Also, as it is shown in the proof of Theorem 4.14 in [57], the inequality $|f^{\rm cl}(x,t)| \leq L|x|$ holds for some positive constant L and all $x \in \mathbb{R}^n$.

In order to analyze the convergence properties of NDOB error dynamics together with the exponentially stabilizing nominal control input $u_{\mathrm{n}}(x,t)$, the candidate Lyapunov function $V(x,e_{\mathrm{d}},t) = V_{\mathrm{n}}(x,t) + V_{\mathrm{d}}(e_{\mathrm{d}})$ is considered. It can be seen from (19) that $c_1|x|^2 + \frac{1}{2}|e_{\mathrm{d}}|^2 \leq V(x,e_{\mathrm{d}},t) \leq c_2|x|^2 + \frac{1}{2}|e_{\mathrm{d}}|^2$. Taking the derivative of V yields the following inequality

$$\dot{V} \leq -\alpha_{\mathrm{d}}|e_{\mathrm{d}}|^2 - c_3|x|^2 + \omega|e_{\mathrm{d}}|. \tag{20}$$

Using Young's inequality, it can be seen that

$$\dot{V} \leq -c_{\mathrm{d}}|e_{\mathrm{d}}|^2 - c_{\mathrm{x}}|x|^2 + \omega_0. \tag{21}$$

where $c_{\mathrm{d}} = \alpha_{\mathrm{d}} - \frac{\omega}{2\epsilon}$, $c_{\mathrm{x}} = c_3$, $\omega_0 = \frac{\epsilon}{2}\omega$, and ϵ is an arbitrary positive constant.

The design parameters α_{d} and ϵ should be chosen such that $c_{\mathrm{d}}, c_{\mathrm{x}} \in \mathbb{R}^+$. It follows from the uniform ultimate boundedness theorems (see "Brief Review of Nonlinear Systems") that for all $x(0) \in \mathbb{R}^n$ and all $e_{\mathrm{d}}(0) \in \mathbb{R}^l$, the disturbance tracking error e_{d} and the state x converge with an exponential rate, proportional to $\min\{c_{\mathrm{d}}, c_{\mathrm{x}}\}$, to a ball centered at the origin with a radius proportional to $\frac{1}{\min\{c_{\mathrm{d}},c_{\mathrm{x}}\}}$.

Comparison with linear DOBs in state-space form

Let the state-space description of a linear system be given by

$$\dot{x} = Ax + B_{\mathrm{u}}u + B_{\mathrm{d}}d,$$
$$y = Cx.$$

Then as it is stated in [10] the dynamical equations of the NDOB (2) reduces to

$$\dot{z} = -L_{\mathrm{d}}B_{\mathrm{d}}(z + Lx) - L_{\mathrm{d}}(Ax + B_{\mathrm{u}}u),$$
$$\hat{d} = z + L_{\mathrm{d}}x,$$

which coincides with the traditional unknown input observers under certain assumptions (see [11]). It can be shown that choosing the constant gain matrix L_{d} such that $-L_{\mathrm{d}}B_{\mathrm{d}}$ is Hurwitz guarantees BIBO stability of the disturbance tracking error. Moreover, when the disturbances are constant, asymptotic convergence of the disturbance tracking error is achieved (see [10] for further details).

Nonlinear Disturbance Observer Design for Euler-Lagrange Systems

In this section, EL systems and their intrinsic dynamic properties are investigated in order to draw more conclusions regarding the capabilities of NDOBs. In particular, a general NDOB gain matrix, which is based on the NDOB structure in [39], [21], is presented for this class of dynamical systems. It is shown that the NDOB gain matrix in [29], which was proposed for serial robotic manipulators, can be used for a more general class of EL systems. Moreover, it is demonstrated how the proposed NDOB can be used along with well-established control schemes such as passivity-based and computed-torque controllers without the need to modify these controllers. Additionally, experimental results are provided to show effectiveness of NDOBs for estimation and rejection of unknown disturbances.

Euler-Lagrange systems and their properties

The model of a *fully actuated* EL system (see "Brief Review of Euler-Lagrange Systems" for further details) with N DOFs and $n = 2N$ states is given by

$$\frac{d}{dt}\frac{\partial \mathcal{L}}{\partial \dot{q}} - \frac{\partial \mathcal{L}}{\partial q} = \tau + \tau_{\mathrm{d}}, \tag{22}$$

where $q \in \mathbb{R}^N$ are the generalized coordinates, $\dot{q} \in \mathbb{R}^N$ are the generalized velocities, $\tau \in \mathbb{R}^N$ is the vector of control inputs, and $\tau_{\mathrm{d}} \in \mathbb{R}^N$ is the lumped disturbance vector. The *Lagrangian* function $\mathcal{L}(q, \dot{q})$ is a smooth function and assumed to have the form [45]

$$\mathcal{L}(q, \dot{q}) = \frac{1}{2}\dot{q}^T M(q)\dot{q} - \mathcal{V}(q), \tag{23}$$

where $M(q) \in \mathbb{R}^{N\times N}$ is the generalized inertia matrix and is assumed to be symmetric and positive definite. Also, $\mathcal{V}(q)$ is the potential function which is assumed to be smooth and bounded from below. Substituting (23) in (22) yields

$$M(q)\ddot{q} + N(q, \dot{q}) = \tau + \tau_{\mathrm{d}}, \tag{24}$$

where,

$$N(q, \dot{q}) = C(q, \dot{q})\dot{q} + G(q), \tag{25}$$

and $C(q,\dot{q})\dot{q} \in \mathbb{R}^N$ is the vector of Coriolis and centrifugal forces. Also, $G(q) := \frac{\partial \mathcal{V}}{\partial q}$ are the forces generated by potential fields such as the gravitational field. As is customary in the robotics literature, the vector $G(q)$ is called the gravity vector in this article.

Following the EL systems literature (see, for example, [58]), it is assumed that the EL model under study has the following properties:

P1

1) The inertia matrix $M(q)$ satisfies

$$\nu_1 I \leq M(q) \leq \nu_2 I, \tag{26}$$

where ν_1 and ν_2 are some positive constants and Inequality (26) holds uniformly with respect to q.

2) The matrix $\dot{M}(q) - 2C(q,\dot{q})$ is skew-symmetric; namely, $z^T\big[\dot{M}(q) - 2C(q,\dot{q})\big]z = 0$ for all $z \in \mathbb{R}^N$.

3) The matrix $C(q,\dot{q})$ is bounded in q and linear in $\dot{q}$; namely,

$$C(q,\dot{q})z = C(q,z)\dot{q}, \tag{27}$$

$$\big|C(q,\dot{q})\big| \leq k_c|\dot{q}|, \tag{28}$$

for all $z \in \mathbb{R}^N$ and some positive constant k_c.

4) Let $q_r \in \mathbb{R}^n$ be an arbitrary vector. There exists a linear parameterization for EL models of the form $M(q)\ddot{q}_{\rm r} + C(q,\dot{q})\dot{q}_{\rm r} + G(q) = \Upsilon(q,\dot{q},\dot{q}_{\rm r},\ddot{q}_{\rm r})\theta$, where Υ is a regressor matrix of known functions and θ is a vector containing EL system parameters.

It is remarked that the EL dynamics (24) can be written in the nonlinear control affine form (1) with

$$\begin{aligned} x &= \begin{bmatrix} q \\ \dot{q} \end{bmatrix} \in \mathbb{R}^n, \\ f(x) &= \begin{bmatrix} \dot{q} \\ M^{-1}(q)\{-C(q,\dot{q})\dot{q} - G(q)\} \end{bmatrix}, \\ g_1(x) &= g_2(x) = \begin{bmatrix} 0 \\ M^{-1}(q) \end{bmatrix}, \end{aligned} \tag{29}$$

where $n = 2N$ is the dimension of the state space.

NDOB structure for EL systems

The lumped disturbance vector $\tau_{\rm d} = \tau_{\rm d}(t)$ in (22) is assumed to satisfy $|\dot{\tau}_{\rm d}| \leq \omega$ for all $t \geq 0$, for some positive constant ω. This class of disturbances includes but is not limited to harmonics and external disturbances.

In EL systems, the NDOB dynamic equations in (2) take the form

$$\begin{aligned} \dot{z} &= -L_{\rm d}(q,\dot{q})z + L_{\rm d}(q,\dot{q})\{N(q,\dot{q}) - \tau - p(q,\dot{q})\}, \\ \hat{\tau}_d &= z + p(q,\dot{q}). \end{aligned} \tag{30}$$

This NDOB was first proposed in [39]; however, no general structure for the observer gain matrix $L_{\rm d}(q,\dot{q})$ was given in that work. Defining the disturbance tracking error to be

$$\Delta\tau_{\rm d} := \hat{\tau}_{\rm d} - \tau_{\rm d},$$

its governing dynamics can be computed as follows

$$\begin{aligned} &\Delta\dot{\tau}_{\rm d} = \dot{\hat{\tau}}_{\rm d} - \dot{\tau}_{\rm d} \underbrace{=}_{(30)} \dot{z} + \dot{p} - \dot{\tau}_{\rm d} = -L_{\rm d}(.)z + L_{\rm d}(.)\big[\underbrace{N(.) - \tau}_{-M(q)\ddot{q}+\tau_{\rm d}} - p(.)\big] + \dot{p}(.) - \dot{\tau}_{\rm d} = \\ &-L_{\rm d}(.)(\hat{\tau}_{\rm d} - p) + L_{\rm d}(.)\big[-M(q)\ddot{q} + \tau_{\rm d} - p(.)\big] + \dot{p}(.) - \dot{\tau}_{\rm d} = -L_{\rm d}(.)\Delta\tau_{\rm d} + \dot{p}(.) \\ &-L_{\rm d}(.)M(q)\ddot{q} - \dot{\tau}_{\rm d} \end{aligned}$$

In order to remove dependence of the disturbance tracking error dynamics on acceleration vector $\ddot{q}$, the relation

$$\frac{d}{dt}p(q,\dot{q}) = L_{\rm d}(q,\dot{q})M(q)\ddot{q}.$$

should hold. On the other hand, $\dot{p}(q,\dot{q}) = \frac{\partial p}{\partial q}\dot{q} + \frac{\partial p}{\partial \dot{q}}\ddot{q}$. Therefore, $\frac{\partial p}{\partial q} = 0$ and $p(.)$ is a function of $\dot{q}$. Also, the relation

$$\frac{\partial p}{\partial \dot{q}} = L_{\rm d}(q,\dot{q})M(q),$$

should hold between the NDOB gain and auxiliary vector. Since $p(.)$ is a function of $\dot{q}$, it necessarily follows that

$$L_{\mathrm{d}}(q,\dot{q}) = A(\dot{q})M^{-1}(q), \tag{31}$$

where $\frac{\partial p}{\partial \dot{q}} = A(\dot{q})$. Therefore, as in [29], the following form may be used for the gain matrix:

$$L_{\mathrm{d}}(q) = X^{-1}M^{-1}(q), \tag{32}$$

where X is a constant symmetric and positive definite $N \times N$ matrix to be determined. For simplicity of exposition, the matrix X is considered to be equal to $\alpha^{-1}I$, where $\alpha = \alpha_{\mathrm{d}}\nu_2$ and ν_2 is the positive constant in Property P1 of EL systems. Using the gain (32), it is seen that

$$p(\dot{q}) = X^{-1}\dot{q}. \tag{33}$$

$$\Delta\dot{\tau}_{\mathrm{d}} = -L_{\mathrm{d}}(q)\Delta\tau_{\mathrm{d}} + \dot{\tau}_{\mathrm{d}}, \tag{34}$$

The following inequality, which is a special case of (7), immediately follows from Property P1 of EL systems and the NDOB gain matrix structure (32), with $X = \alpha^{-1}I$,

$$-\Delta\tau_{\mathrm{d}}^T L_{\mathrm{d}}(q)\Delta\tau_{\mathrm{d}} \leq -\alpha_{\mathrm{d}}|\Delta\tau_{\mathrm{d}}|^2, \text{ for all } q \in \mathbb{R}^N,\ \Delta\tau_{\mathrm{d}} \in \mathbb{R}^N. \tag{35}$$

Augmented dynamics of EL systems with NDOBs

In this section, the properties of augmented EL system (24) with NDOB (30),(32) and the add-on feature of the NDOB are studied. In order to suppress the adverse effects of disturbances, the following NDOB-based control input is applied to the EL system

$$\tau = \tau_{\mathrm{n}} - \hat{\tau}_{\mathrm{d}}, \tag{36}$$

where $\tau_{\rm n}$ is the nominal control input and $\hat{\tau}_{\rm d}$ is the estimated lumped disturbance generated by NDOB (30). It follows that the augmented EL dynamics with NDOB (30) and control input (36) read as

$$\begin{aligned} M(q)\ddot{q} + N(q,\dot{q}) &= \tau_{\rm n} - \Delta\tau_{\rm d}, \\ \Delta\dot{\tau}_d &= -\alpha M^{-1}(q)\Delta\tau_{\rm d} + \dot{\tau}_d. \end{aligned} \tag{37}$$

Semi/Quasi-passivity property of augmented EL systems with NDOBs

In this section, it is assumed that the nominal control input $\tau_{\rm n}$ has the form of conventional passivity-based controllers designed for EL systems; namely, it can be written as

$$\tau_{\rm n} = \tau_{\rm np} + G(q). \tag{38}$$

In order to analyze the behavior of the augmented EL system and NDOB in (37), the following *storage function* (see "Brief Review of Nonlinear Systems") is considered

$$V = \frac{1}{2}\dot{q}^T M(q)\dot{q} + \frac{1}{2}\Delta\tau_{\rm d}^T\Delta\tau_{\rm d}. \tag{39}$$

Taking the derivative of (39) along the trajectories of the system (37) and using Property P2 of EL systems, it can be shown that

$$\dot{V} = \dot{q}^T\tau_{\rm np} - \alpha\Delta\tau_{\rm d}^T M^{-1}(q)\Delta\tau_{\rm d} + \Delta\tau_{\rm d}^T\dot{\tau}_{\rm d}. \tag{40}$$

Using Young's inequality along with properties P1 and P3 of EL systems in Equation (40) yields

$$\dot{V} \leq \dot{q}^T\tau_{\rm np} - \underbrace{\left[c_{\rm d}|\Delta\tau_{\rm d}|^2 - \frac{\omega\epsilon}{2}\right]}_{H(\Delta\tau_{\rm d})}, \tag{41}$$

where ϵ is some positive constant, and

$$c_{\rm d} = \alpha_{\rm d} - \frac{\omega}{2\epsilon}. \tag{42}$$

The design parameters $\alpha_{\rm d}$ and ϵ should be chosen such that $c_{\rm d}$ becomes positive.

It follows from the Inequality (41) that the augmented EL system with NDOB (37) is semi/quasi-passive (see "Brief Review of Nonlinear Systems"). It is remarked that this observation has not been reported in the previous NDOB literature. One of the significant implications of this observation is that the NDOB (30) with gain (32) can be used along with any control scheme that exploits the passivity property of EL systems since the augmented EL system with the proposed NDOB is guaranteed to be semi/quasi-passive. It is remarked that this NDOB possesses the add-on feature since there is no need to modify the previously designed passivity-based controllers for EL systems along with this NDOB.

Properties of augmented EL systems with NDOBs controlled by computed-torque/feedback linearizing schemes

In this section, the uniform ultimate boundedness property of NDOBs along with exponentially stabilizing control schemes, which was discussed in the general NDOB section, is used to investigate the add-on feature of the NDOB (30) with gain (32) along with the well-established trajectory tracking computed-torque/feedback linearizing schemes.

The vectors $q_{\rm r}(t) \in \mathbb{R}^N$ and $e_{\rm r}(t) := q(t) - q_{\rm r}(t)$ are considered to represent desired smooth trajectories for the generalized coordinates of the EL system, and the trajectory tracking error, respectively. The nominal control input $\tau_{\rm n}$ in (36) is considered to be the computed-torque control law

$$\tau_{\rm n} = M(q)\{\ddot{q}_{\rm r} + N(q,\dot{q}) - K_{\rm p} e_{\rm r} - K_{\rm d}\dot{e}_{\rm r}\}, \tag{43}$$

where the matrices $K_{\rm p}$ and $K_{\rm d}$ are chosen such that the origin $(e_{\rm r}, \dot{e}_{\rm r}) = (0,0)$ of the closed-loop trajectory tracking error dynamics

$$\ddot{e}_{\rm r} + K_{\rm d}\dot{e}_{\rm r} + K_{\rm p} e_{\rm r} = 0, \tag{44}$$

is exponentially stable. Using the nominal control law (43) in (36) result in the closed-loop augmented dynamics

$$\ddot{e}_{\rm r} + K_{\rm d}\dot{e}_{\rm r} + K_{\rm p}e_{\rm r} = -M^{-1}(q)\Delta\tau_{\rm d},$$
$$\Delta\dot{\tau}_{\rm d} = -\alpha M^{-1}(q)\Delta\tau_{\rm d} + \dot{\tau}_{\rm d}. \tag{45}$$

It is to be noted that the augmented closed-loop dynamics (45) are analogous to the dynamics that were investigated in Section "Uniform ultimate boundedness of NDOBs". Therefore, the Lyapunov stability analysis can be carried out completely similar to the analysis in the aforementioned section. From Equation (21) and the uniform ultimate boundedness theorem (see "Brief Review of Nonlinear Systems") that for all $e_{\rm r}(0), \dot{e}_{\rm r}(0) \in \mathbb{R}^N$ and all $\Delta\tau_{\rm d}(0) \in \mathbb{R}^N$, the tracking error $\Delta\tau_{\rm d}$ and the states $e_{\rm r}, \dot{e}_{\rm r}, \Delta\tau_{\rm d}$ converge with an exponential rate to a ball centered at the origin with a radius that can be as small as possible by properly choosing the design parameters.

Experimental results

This section demonstrates experimental results regarding the NDOB-based control for a PHANToM Omni haptic device (see "PHANToM Omni and its Parameter Identification"). The PHANToM Omni has three actuated revolute joints which provide the user with force feedback information. In addition to the actuated joints, the PHANToM robot has three wrist joints that are passive. The first and the third actuated joints of the PHANToM robot in experiments will be used while the second actuated joint is locked at $0^{\rm deg}$. It is to noted that this mechanism is not confined to a constant 2-D plane and moves in three-dimensional space. Therefore, the NDOB gain proposed by [39] or [28] cannot be employed here. The PHANToM Omni is connected to the computer through an IEEE 1394 port. The PHANToM Omni end-effector position and orientation data are collected at a frequency of 1 kHz. The NDOB is used to estimate and compensate for the joint frictions and external payload. The payload is a metal cube which is attached to the gimbal of the robot. In order to employ the computed-torque scheme in this experiment, the PHANToM parameters were identified (see "PHANToM Omni and its Parameter Identification").

Sinusoidal commands are supplied as the reference trajectory for the first and the third joints of the robot in the presence of the computed-torque control scheme (43). The experiments are performed in three different cases, namely, with no DOB, with the DOB given in [14], and with the NDOB proposed in [39], [22] with NDOB gain given in [29].

The proportional and derivative gains are chosen to be equal to $1.4I$ and $0.5I$, respectively. The DOB gain matrix of observer in [14] has been chosen to be I. In addition, the disturbance tracking performance of the proposed DOB in the article is compared with that of employed by

TABLE 2: Experimental study: Joint trajectory tracking error root mean square (RMS) values. The nonlinear disturbance observer (NDOB), accompanying the computed-torque controller in this experiment, is used to estimate and compensate for the joint frictions and external payload. The payload is a metal cube which is attached to the gimbal of the robot. The main disturbance in this experiment is due to the external payload that (see "PHANToM Omni and its Parameter Identification") affects only the third joint of the robot. According to this table, the root mean square (RMS) position tracking error of the third joint has been significantly improved using the NDOB structure of [21], [39] with NDOB gain given in [29].

	No DOB	DOB given in [14]	NDOB given in [21], [29]
RMS Error Joint 1	2.02×10^{-2}	1.19×10^{-2}	9.98×10^{-3}
RMS Error Joint 3	1.23×10^{-1}	7.69×10^{-2}	3.31×10^{-2}

TABLE 3: Experimental study: Disturbance tracking error root mean square (RMS) values. The nonlinear disturbance observer (NDOB), accompanying the computed-torque controller in this experiment, is used to estimate and compensate for the joint frictions and external payload. The payload is a metal cube which is attached to the gimbal of the robot. The main disturbance in this experiment is due to the external payload that (see "PHANToM Omni and its Parameter Identification") affects only the third joint of the robot. According to this table, the root mean square (RMS) disturbance tracking errors have been significantly improved using the NDOB structure of [21], [39] with NDOB gain given in [29].

	DOB given in [14]	DOB given in [60]	NDOB given in [21], [29]
RMS Error Joint 1	9.85×10^{-3}	1.44×10^{-2}	5.52×10^{-3}
RMS Error Joint 3	1.42×10^{-2}	2.02×10^{-2}	1.00×10^{-2}

[14] and [60]. The DOB given by [60] is the conventional LDOB that has been employed in numerous robotic applications (see, for example, [61], [16], [62]). The parameters of the DOB in [60] have been chosen to be $g_{\text{reac}} = 100$ and $K_{\text{tn}} = 1$.

Figures 6, 7, 8, and 9 illustrate the time profiles of positions and tracking errors of joints 1 and 3, respectively. Table 2 contains the RMS values of joint tracking errors. Figures 10 and 11 illustrate the time profiles of disturbances and disturbance tracking errors of joints 1 and 3, respectively. Table 3 contains the RMS values of disturbance tracking errors. Note that the identification of the dynamic model of the robot was not perfect. Therefore, the NDOB compensates the effect of dynamic uncertainties that exist in the model of the robot. The tracking error is guaranteed to be bounded and to converge to its ultimate bound region with an exponential rate. As it can be seen from Tables 2 and 3, the disturbance and position tracking performance of the NDOB in [39], [21] with the gain given by [29] excels the performance of that of proposed by [14] and [60].

Application of NDOBs in Teleoperation

In this section, applications of NDOBs in teleoperation systems are discussed. In particular, NDOBs are incorporated in a well-known architecture that is capable of achieving transparency in the absence of disturbances [52]. It is shown that NDOBs can recover the performance of the 4-channel architecture in the presence of disturbances. The conventional 4-channel architecture requires acceleration measurements for achieving transparency in the absence of disturbances. These additional measurements can be used in order to simplify the NDOB structure which was introduced in the previous section. The dynamical models investigated for the 4-channel architecture and the proposed NDOBs are described in the Cartesian space. This approach makes the teleoperation system stable and transparent where there is a need for the end-effector of the robots to have synchronized pose (position and orientation).

4-channel transparent teleoperation

Given the generalized coordinates, generalized velocities, and dynamic equations in the joint space, a coordinate transformation is required to obtain their counterparts in the Cartesian space. The Jacobian matrix of a single robot and the position/orientation (pose) vector of the robot's end-effector in the Cartesian space are denoted by $J(q)$ and x, respectively. It is assumed that J is of full column rank; in other words, the robot is not at a singularity and $J_* = J^T J$ is invertible. Using $\dot{x} = J\dot{q}$ and $\ddot{x} = \dot{J}\dot{q} + J\ddot{q}$ in (24), the following dynamic equation is obtained

$$M_{\mathrm{x}}(q)\ddot{x} + N_{\mathrm{x}}(q,\dot{q}) = f + f_d, \tag{46}$$

where,

$$\begin{aligned} M_{\mathrm{x}}(q) &= JJ_*^{-1}M(q)J_*^{-1}J^T, & (47)\\ N_{\mathrm{x}}(q,\dot{q}) &= JJ_*^{-1}N(q,\dot{q}) - M_{\mathrm{x}}(q)\dot{J}J_*^{-1}J^T\dot{x}, & (48) \end{aligned}$$

and

$$\begin{aligned} f &= JJ_*^{-1}\tau, & (49)\\ f_{\mathrm{d}} &= JJ_*^{-1}\tau_{\mathrm{d}}. & (50) \end{aligned}$$

Equation (46) governs the motion of the end-effector of the robot in the Cartesian space. Similarly, the dynamic equations governing the pose of the end-effectors of the master and slave robots, which are interacting with the human operator and the remote environment in the presence of disturbances, can be written as

$$M_{\mathrm{xm}}(q_{\mathrm{m}})\ddot{x}_{\mathrm{m}} + N_{\mathrm{xm}}(q_{\mathrm{m}}, \dot{q}_{\mathrm{m}}) = f_{\mathrm{m}} + f_{\mathrm{h}} + f_{\mathrm{d,m}}, \tag{51}$$

$$M_{\mathrm{xs}}(q_{\mathrm{s}})\ddot{x}_{\mathrm{s}} + N_{\mathrm{xs}}(q_{\mathrm{s}}, \dot{q}_{\mathrm{s}}) = f_{\mathrm{s}} - f_{\mathrm{e}} + f_{\mathrm{d,s}}, \tag{52}$$

where q_{m}, q_{s}, x_{m}, x_{s}, $M_{\mathrm{xm}}(q_{\mathrm{m}})$, $M_{\mathrm{xs}}(q_{\mathrm{s}})$, $N_{\mathrm{xm}}(q_{\mathrm{m}}, \dot{q}_{\mathrm{m}})$ and $N_{\mathrm{xs}}(q_{\mathrm{s}}, \dot{q}_{\mathrm{s}})$ are defined as in (46) and subscripts m and s refer to the master and the slave, respectively. Also, $f_{\mathrm{m}}, f_{\mathrm{s}} \in \mathbb{R}^{6\times 1}$ are the (equivalent) control forces applied to the master and the slave end-effectors in the Cartesian space, $f_{\mathrm{h}}, f_{\mathrm{e}} \in \mathbb{R}^{6\times 1}$ are the forces exerted to the master and the slave end-effectors by the human operator and the remote environment, and $f_{\mathrm{d,m}}, f_{\mathrm{d,s}} \in \mathbb{R}^{6\times 1}$ are the (equivalent) disturbance forces exerted to the master and the slave end-effectors in the Cartesian space. These disturbance forces represent the lumped effect of disturbances exerted to the master and the slave robots in the Cartesian space.

The 4-channel control architecture is shown in Figure 12 with DOBs incorporated into it. Exogenous signals f_{h}^* and f_{e}^* are exerted by the human operator and the remote environment, respectively. The signals x_{m}, x_{s}, f_{h}, f_{e}, f_{m}, f_{s}, $f_{\mathrm{d,m}}$ and $f_{\mathrm{d,s}}$ are as defined in (51)–(52). Position and force information are exchanged between the two robots via the position channels C_1, C_4, and the force channels C_2, C_3, respectively. Moreover, C_{m} and C_{s} are local master and slave (position) controllers. Finally, local force feedback from the human operator and the remote environment are provided by C_5 and C_6 to the master and the slave, respectively.

Closed-loop stability and transparency are the two essential control requirements for every teleoperation system [52]. In a fully transparent teleoperation system, perfect position and force tracking are achieved, namely, $x_{\mathrm{s}} = x_{\mathrm{m}}$ and $f_{\mathrm{h}} = f_{\mathrm{e}}$ hold, respectively. If the master and the slave can be modeled by LTI impedances, namely, causal dynamic operators which map position/velocity to force, $Z_{\mathrm{m}}(s)$ and $Z_{\mathrm{s}}(s)$, the 4-channel teleoperation system of Figure 12, when no DOB is incorporated into it, becomes fully transparent in the absence of disturbances and delays if the controllers are chosen as [53]

$$
\begin{aligned}
C_1 &= Z_{\mathrm{s}} + C_{\mathrm{s}}, \\
C_2 &= I + C_6, \\
C_3 &= I + C_5, \\
C_4 &= -Z_{\mathrm{m}} - C_{\mathrm{m}}.
\end{aligned} \tag{53}
$$

Extending the idea of DOB-based control of a single robot to a master-slave teleoperation system, a DOB for each of the master and slave robots are designed in order to estimate and cancel out the disturbances. The 4-channel architecture with NDOBs incorporated into it are shown in Figure 12.

The vectors $\hat{f}_{\mathrm{d,m}}$ and $\hat{f}_{\mathrm{d,s}}$ denote the master and slave disturbance estimates, respectively. These estimates are employed in a feedforward manner in the following nonlinear control laws for the master and slave robots described by (51) and (52), respectively:

$$
\begin{aligned}
f_{\mathrm{m}} &= M_{\mathrm{xm}}(q_{\mathrm{m}})[-C_{\mathrm{m}}x_{\mathrm{m}} - C_2 f_{\mathrm{e}} - C_4 x_{\mathrm{s}} + C_6 f_{\mathrm{h}} + f_{\mathrm{h}}] \\
&\quad + N_{\mathrm{xm}}(q_{\mathrm{m}}, \dot{q}_{\mathrm{m}}) - f_{\mathrm{h}} - \hat{f}_{\mathrm{d,m}}, \qquad (54) \\
f_{\mathrm{s}} &= M_{\mathrm{xs}}(q_{\mathrm{s}})[-C_{\mathrm{s}}x_{\mathrm{s}} + C_1 x_{\mathrm{m}} + C_3 f_{\mathrm{h}} - C_5 f_{\mathrm{e}} - f_{\mathrm{e}}] \\
&\quad + N_{\mathrm{xs}}(q_{\mathrm{s}}, \dot{q}_{\mathrm{s}}) + f_{\mathrm{e}} - \hat{f}_{\mathrm{d,s}}, \qquad (55)
\end{aligned}
$$

where C_{m}, C_{s}, C_1, $\ldots$, and C_6 are some LTI controllers satisfying the transparency condition in (53).

The DOB-based control laws (54) and (55), when applied to the master and slave described by (51)–(52), yield the following closed-loop equations for the master and slave:

$$
\begin{aligned}
\ddot{x}_{\mathrm{m}} &= -C_{\mathrm{m}}x_{\mathrm{m}} - C_2 f_{\mathrm{e}} - C_4 x_{\mathrm{s}} + C_6 f_{\mathrm{h}} \\
&\quad + f_{\mathrm{h}} + M_{\mathrm{xm}}^{-1}(q_{\mathrm{m}})\Delta f_{\mathrm{d,m}}, \qquad (56) \\
\ddot{x}_{\mathrm{s}} &= -C_{\mathrm{s}}x_{\mathrm{s}} + C_1 x_{\mathrm{m}} + C_3 f_{\mathrm{h}} - C_5 f_{\mathrm{e}} \\
&\quad - f_{\mathrm{e}} + M_{\mathrm{xs}}^{-1}(q_{\mathrm{s}})\Delta f_{\mathrm{d,s}}, \qquad (57)
\end{aligned}
$$

where $\Delta f_{\mathrm{d,m}} = f_{\mathrm{d,m}} - \hat{f}_{\mathrm{d,m}}$ and $\Delta f_{\mathrm{d,s}} = f_{\mathrm{d,s}} - \hat{f}_{\mathrm{d,s}}$ are the master and the slave disturbance estimation errors, respectively. Under perfect disturbance tracking, namely, when $\Delta f_{\mathrm{d,m}} = 0$

and $\Delta f_{\mathrm{d,s}} = 0$, (56) and (57) describe an N-DOF conventional disturbance-free 4-channel teleoperation system where the master and slave robots are given by identity inertia matrices, namely, $Z_{\mathrm{m}}(s) = s^2 I$ and $Z_{\mathrm{s}}(s) = s^2 I$.

When the master and slave local position controllers in (54) and (55) are of proportional-derivative type, then

$$\begin{aligned} C_{\mathrm{m}} &= K_{\mathrm{mv}} s + K_{\mathrm{mp}}, \\ C_{\mathrm{s}} &= K_{\mathrm{sv}} s + K_{\mathrm{sp}}, \end{aligned} \tag{58}$$

where K_{mv}, K_{mp}, K_{sv} and K_{sp} are constant gain matrices. Also, the force reflection gains in (54) and (55) are chosen to be

$$\begin{aligned} C_2 &= C_{\mathrm{mf}}, \\ C_3 &= C_{\mathrm{sf}}, \end{aligned} \tag{59}$$

where C_{mf} and C_{sf} are constant force reflection gain matrices. The other controllers in (54) and (55) are chosen to satisfy the full transparency conditions given by (53). Accordingly,

$$\begin{aligned} C_1 &= s^2 I + K_{\mathrm{sv}} s + K_{\mathrm{sp}}, \\ C_4 &= -(s^2 I + K_{\mathrm{mv}} s + K_{\mathrm{mp}}), \\ C_5 &= C_{\mathrm{sf}} - I, \\ C_6 &= C_{\mathrm{mf}} - I. \end{aligned} \tag{60}$$

Implementing the controllers C_1 and C_4 in (60) require measurement or computation of acceleration of the master and slave robots. When only good low-frequency transparency is enough for the desired application, the acceleration terms can be omitted. However, requiring good transparency over both low and high frequencies justifies using accelerometers [52]. Alternatively, precise numerical differentiation techniques may be employed, which are robust to measurement errors and input noises, in order to obtain acceleration and velocity signals from position measurements [63].

Using (58), (59), and (60) in (54)–(55) yields the control laws

$$
\begin{aligned}
f_{\mathrm{m}} &= M_{\mathrm{xm}}(q_{\mathrm{m}})[\ddot{x}_{\mathrm{s}} - K_{\mathrm{mv}}\Delta\dot{x} - K_{\mathrm{mp}}\Delta x + C_{\mathrm{mf}}\Delta f] \\
&\quad + N_{\mathrm{xm}}(q_{\mathrm{m}}, \dot{q}_{\mathrm{m}}) - f_{\mathrm{h}} - \hat{f}_{\mathrm{d,m}}, \qquad (61) \\
f_{\mathrm{s}} &= M_{\mathrm{xs}}(q_{\mathrm{s}})[\ddot{x}_{\mathrm{m}} + K_{\mathrm{sv}}\Delta\dot{x} + K_{\mathrm{sp}}\Delta x + C_{\mathrm{sf}}\Delta f] \\
&\quad + N_{\mathrm{xs}}(q_{\mathrm{s}}, \dot{q}_{\mathrm{s}}) + f_{\mathrm{e}} - \hat{f}_{\mathrm{d,s}}, \qquad (62)
\end{aligned}
$$

where $\Delta x = x_{\mathrm{m}} - x_{\mathrm{s}}$ and $\Delta f = f_{\mathrm{h}} - f_{\mathrm{e}}$ are the position and force tracking errors, respectively. Under the control laws (61) and (62), the master and slave closed-loop dynamics (56) and (57) are governed by

$$
\begin{aligned}
\Delta\ddot{x} &= -K_{\mathrm{mv}}\Delta\dot{x} - K_{\mathrm{mp}}\Delta x + C_{\mathrm{mf}}\Delta f + M_{\mathrm{xm}}^{-1}(q_{\mathrm{m}})\Delta f_{\mathrm{d,m}} \qquad (63) \\
\Delta\ddot{x} &= K_{\mathrm{sv}}\Delta\dot{x} + K_{\mathrm{sp}}\Delta x - C_{\mathrm{sf}}\Delta f - M_{\mathrm{xs}}^{-1}(q_{\mathrm{s}})\Delta f_{\mathrm{d,s}} \qquad (64)
\end{aligned}
$$

It is assumed that matrices C_{mf}, C_{sf} and $C_{\mathrm{mf}}^{-1} + C_{\mathrm{sf}}^{-1}$ are invertible. Consequently, multiplying (63) and (64) by C_{mf}^{-1} and C_{sf}^{-1}, respectively and adding them together, the dynamic equation governing the position tracking error reads as

$$
\Delta\ddot{x} + K_{\mathrm{v}}\Delta\dot{x} + K_{\mathrm{p}}\Delta x = \Psi_{\mathrm{xm}}(q_{\mathrm{m}})\Delta f_{\mathrm{d,m}} - \Psi_{\mathrm{xs}}(q_{\mathrm{s}})\Delta f_{\mathrm{d,s}}, \qquad (65)
$$

where

$$
\begin{aligned}
K_{\mathrm{v}} &= (C_{\mathrm{mf}}^{-1} + C_{\mathrm{sf}}^{-1})^{-1}(C_{\mathrm{sf}}^{-1}K_{\mathrm{sv}} - C_{\mathrm{mf}}^{-1}K_{\mathrm{mv}}) \qquad (66) \\
K_{\mathrm{p}} &= (C_{\mathrm{mf}}^{-1} + C_{\mathrm{sf}}^{-1})^{-1}(C_{\mathrm{sf}}^{-1}K_{\mathrm{sp}} - C_{\mathrm{mf}}^{-1}K_{\mathrm{mp}}), \\
\Psi_{\mathrm{xm}}(q_{\mathrm{m}}) &= (C_{\mathrm{mf}}^{-1} + C_{\mathrm{sf}}^{-1})^{-1}C_{\mathrm{mf}}^{-1}M_{\mathrm{xm}}^{-1}(q_{\mathrm{m}}) \qquad (67) \\
\Psi_{\mathrm{xs}}(q_{\mathrm{s}}) &= (C_{\mathrm{mf}}^{-1} + C_{\mathrm{sf}}^{-1})^{-1}C_{\mathrm{sf}}^{-1}M_{\mathrm{xs}}^{-1}(q_{\mathrm{s}}), . \qquad (68)
\end{aligned}
$$

As mentioned before, the need for full transparency in a wide frequency range that is required by the transparency conditions in (53) for use in (61) and (62) justifies using accelerometers. Consequently, the acceleration measurements, which are used by the conventional

4-channel controllers, are employed in order to simplify NDOB design. Given the master and slave dynamics (51)–(52), the following NDOBs are employed in the 4-channel teleoperation architecture

$$\begin{aligned}\dot{\hat{f}}_{\mathrm{d,m}} &= -L_{\mathrm{m}}\hat{f}_{\mathrm{d,m}} + L_{\mathrm{m}}[M_{\mathrm{xm}}(q_{\mathrm{m}})\ddot{x}_{\mathrm{m}} + N_{\mathrm{xm}}(q_{\mathrm{m}},\dot{q}_{\mathrm{m}}) \\ &\quad -f_{\mathrm{h}} - f_{\mathrm{m}}] + \Psi_{\mathrm{xm}}^{T}(q_{\mathrm{m}})(\Delta\dot{x} + \gamma\Delta x), \qquad (69)\\ \dot{\hat{f}}_{\mathrm{d,s}} &= -L_{\mathrm{s}}\hat{f}_{\mathrm{d,s}} + L_{\mathrm{s}}[M_{\mathrm{xs}}(q_{\mathrm{s}})\ddot{x}_{\mathrm{s}} + N_{\mathrm{xs}}(q_{\mathrm{s}},\dot{q}_{\mathrm{s}}) \\ &\quad +f_{\mathrm{e}} - f_{\mathrm{s}}] + \Psi_{\mathrm{xs}}^{T}(q_{\mathrm{s}})(-\Delta\dot{x} - \gamma\Delta x), \qquad (70)\end{aligned}$$

where γ is an arbitrary positive constant. Also, L_{m} and L_{s} are constant gain matrices. As it can be seen from (69) and (70), NDOB gains L_{m} and L_{s} are constant and there is no need for the auxiliary vector $p(.)$ in the NDOB dynamics. It is remarked that knowing the acceleration signals from accelerometers that are employed in the conventional 4-channel teleoperation simplifies the structure of NDOB gain matrices in comparison with the NDOB structure used in the previous sections.

In the conventional 4-channel teleoperation control architecture, human and environmental forces, namely, f_{h} and f_{e}, are measured. Equations (51) and (52), along with (69) and (70), result in the following disturbance estimation error dynamics:

$$\begin{aligned}\dot{\tilde{f}}_{\mathrm{d,m}} &= L_{\mathrm{m}}\Delta f_{\mathrm{d,m}} + \Psi_{\mathrm{xm}}^{T}(q_{\mathrm{m}})(\Delta\dot{x} + \gamma\Delta x), \qquad (71)\\ \dot{\tilde{f}}_{\mathrm{d,s}} &= L_{\mathrm{s}}\Delta d_{\mathrm{s}} + \Psi_{\mathrm{xs}}^{T}(q_{\mathrm{s}})(-\Delta\dot{x} - \gamma\Delta x). \qquad (72)\end{aligned}$$

Therefore, the following disturbance estimation error dynamics result from (71) and (72) for the master and the slave, respectively:

$$\begin{aligned}\Delta\dot{f}_{\mathrm{d,m}} &= \dot{f}_{\mathrm{d,m}} - L_{\mathrm{m}}\Delta f_{\mathrm{d,m}} - \underbrace{\Psi_{\mathrm{xm}}^{T}(q_{\mathrm{m}})(\Delta\dot{x} + \gamma\Delta x)}_{\zeta_{\mathrm{m}}}, \qquad (73)\\ \Delta\dot{f}_{\mathrm{d,s}} &= \dot{f}_{\mathrm{d,s}} - L_{\mathrm{s}}\Delta f_{\mathrm{d,s}} - \underbrace{\Psi_{\mathrm{xs}}^{T}(q_{\mathrm{s}})(-\Delta\dot{x} - \gamma\Delta x)}_{\zeta_{\mathrm{s}}}. \qquad (74)\end{aligned}$$

It is remarked that the terms $\zeta_{\mathrm{m}} = \Psi_{\mathrm{xm}}^{T}(q_{\mathrm{m}})(\Delta\dot{x} + \gamma\Delta x)$ and $\zeta_{\mathrm{s}} = \Psi_{\mathrm{xs}}^{T}(q_{\mathrm{s}})(-\Delta\dot{x} - \gamma\Delta x)$ are employed in the NDOBs in order to improve the performance of the teleoperation system.

To analyze the performance of this NDOB-based 4-channel architecture, the candidate Lyapunov function

$$V(\Delta\dot{x}, \Delta x, \Delta d_{\mathrm{m}}, \Delta d_{\mathrm{s}}) = \frac{1}{2}(\Delta\dot{x} + \gamma\Delta x)^T(\Delta\dot{x} + \gamma\Delta x)$$
$$+\frac{1}{2}\Delta x^T(K_{\mathrm{p}} + \gamma K_{\mathrm{v}} - \gamma^2 I)\Delta x + \frac{1}{2}\Delta d_{\mathrm{m}}^T\Delta d_{\mathrm{m}} + \frac{1}{2}\Delta d_{\mathrm{s}}^T\Delta d_{\mathrm{s}},$$

is considered. Taking its derivative yields

$$\dot{V} \leq -\kappa_0|e|^2 + \xi_0|e|, \tag{75}$$

where $e = [\Delta\dot{x}^T, \Delta x^T, \Delta f_{\mathrm{d,m}}^T, \Delta f_{\mathrm{d,s}}^T]^T$, $\kappa_0 = \min\{\lambda_{\min}(K_{\mathrm{v}} - \gamma I), \gamma\lambda_{\min}(K_{\mathrm{p}}), \lambda_{\min}(L_{\mathrm{m}}), \lambda_{\min}(L_{\mathrm{s}})\}$, and ξ_0 is some constant that is proportional to the rate of change of the lumped disturbances $f_{\mathrm{d,m}}$ and $f_{\mathrm{d,s}}$ (see [49] for further details). It immediately follows that the disturbance and position tracking errors of the teleoperation system are globally uniformly ultimately bounded (see "Brief Review of Nonlinear Systems") and converge with an exponential rate proportional to κ_0 to an open ball centered at the origin with a radius proportional to $\frac{1}{\kappa_0}$. Since κ_0 can be made arbitrarily large by tuning the design parameters, the 4-channel teleoperation architecture using NDOBs is practically stable.

NDOB-based 4-channel teleoperation simulations

In this section, computer simulations will illustrate effectiveness of the proposed NDOB in 4-channel teleoperation subject to disturbances. Both the master and slave robots are considered to be planar two-link manipulators with revolute joints. Figure 13 depicts schematic diagram of the teleoperation system.

The Cartesian dynamics of the manipulators are described by [64]

$$M_x(q) = \begin{bmatrix} m_2 + \frac{m_1}{s_2^2} & 0 \\ 0 & m_2 \end{bmatrix},$$

$$V_x(q, \dot{q}) = \begin{bmatrix} V_{\mathrm{x}_1}(q, \dot{q}) \\ V_{\mathrm{x}_2}(q, \dot{q}) \end{bmatrix},$$

$$G_x(q) = \begin{bmatrix} m_1 g \frac{c_1}{s_2} + m_2 g s_{12} \\ m_2 g c_{12} \end{bmatrix},$$

where

$$\begin{aligned} V_{\mathrm{x}_1} &= -(m_2 l_1 c_2 + m_2 l_2)\dot{q}_1^2 - m_2 l_2 \dot{q}_2^2 - \\ &\quad (2m_2 l_2 + m_2 l_1 c_2 + m_1 l_1 \frac{c_2}{s_2^2})\dot{q}_1 \dot{q}_2, \\ V_{\mathrm{x}_2} &= m_2 l_1 s_2 \dot{q}_1^2 + l_1 m_2 s_2 \dot{q}_1 \dot{q}_2. \end{aligned}$$

Also, the forward kinematics and the Jacobian matrix are

$$h(q) = \begin{bmatrix} l_1 c_1 + l_2 c_{12} \\ l_1 s_1 + l_2 s_{12} \end{bmatrix},$$

$$J(q) = \begin{bmatrix} l_1 s_2 & 0 \\ l_1 c_2 + l_2 & l_2 \end{bmatrix},$$

where l_1 and l_2 are the lengths of the links, and m_1 and m_2 are the point masses of the links. Moreover, the abbreviations $s_1 = \sin(q_1)$, $s_2 = \sin(q_2)$, $c_1 = \cos(q_1)$, $c_2 = \cos(q_2)$, $s_{12} = \sin(q_1 + q_2)$ and $c_{12} = \cos(q_1 + q_2)$ are used in the aforementioned dynamic equations.

In this simulation study, the human operator's hand and remote environment are modeled as second-order LTI systems. Accordingly,

$$\begin{aligned} f_{\mathrm{h}} &= f_{\mathrm{h}}^* - (M_{\mathrm{h}} \ddot{x}_{\mathrm{m}} + B_{\mathrm{h}} \dot{x}_{\mathrm{m}} + K_{\mathrm{h}} x_{\mathrm{m}}), \\ f_{\mathrm{e}} &= f_{\mathrm{e}}^* + M_{\mathrm{e}} \ddot{x}_{\mathrm{s}} + B_{\mathrm{e}} \dot{x}_{\mathrm{s}} + K_{\mathrm{e}} x_{\mathrm{s}}, \end{aligned}$$

where $M_{\mathrm{h}} = m_{\mathrm{h}} I$, $M_{\mathrm{e}} = m_{\mathrm{e}} I$, $B_{\mathrm{h}} = b_{\mathrm{h}} I$, $B_{\mathrm{e}} = b_{\mathrm{e}} I$, $K_{\mathrm{h}} = k_{\mathrm{h}} I$ and $K_{\mathrm{e}} = k_{\mathrm{e}} I$ are the mass, damping, and stiffness coefficients of the envirnoment and the human operator's hand, and I is the identity matrix. Also, f_{h}^* and f_{e}^* represent the human and the environment exogenous forces, respectively. The overall human hand parameters have been measured in several papers such as

[65], [66] and [67]. In the simulations, the human hand parameters are chosen as in [66]. The remote environment is modeled by dampers and springs. Accordingly,

$$m_{\mathrm{h}} = 11.6kg,\ b_{\mathrm{h}} = 17Nsm^{-1},\ k_{\mathrm{h}} = 243Nm^{-1},$$
$$b_{\mathrm{e}} = 5Nsm^{-1},\ k_{\mathrm{e}} = 1Nm^{-1}.$$

The friction torques acting on the joints of the robots are generated based on the model in [68]. For the i^{th} joint of the robot, $i = 1,\ 2$, the frictions can be modeled as

$$\begin{aligned}\tau_{\mathbf{i}_{\mathbf{friction}}} &= F_{\mathbf{ci}}\mathrm{sgn}(\dot{q}_{\mathrm{i}})[1-\exp(\frac{-\dot{q}_{\mathrm{i}}^2}{v_{\mathbf{si}}^2})] \\ &\quad + F_{\mathbf{si}}\mathrm{sgn}(\dot{q}_{\mathrm{i}})\exp(\frac{-\dot{q}_{\mathrm{i}}^2}{v_{\mathbf{si}}^2}) + F_{\mathbf{vi}}\dot{q}_{\mathrm{i}},\end{aligned}$$

where F_{ci}, F_{si}, F_{vi} are the Coulomb, static, and viscous friction coefficients, respectively. The parameter v_{si} is the Stribeck parameter. In the simulations, the friction coefficients and the Stribeck parameter for the master and the slave are chosen as follows [69]:

$$F_{\mathrm{ci}} = 0.49,\ F_{\mathrm{si}} = 3.5,\ F_{\mathrm{vi}} = 0.15,\ v_{\mathrm{si}} = 0.189,\ i = 1, 2.$$

The actual parameter values of the master and the slave robots are taken to be

$$m_{1\mathrm{m}} = 2.3kg,\ m_{2\mathrm{m}} = 2.3kg,\ l_{1\mathrm{m}} = 0.5m,\ l_{2\mathrm{m}} = 0.5m,$$
$$m_{1\mathrm{s}} = 1.5kg,\ m_{2\mathrm{s}} = 1.5kg,\ l_{1\mathrm{s}} = 0.5m,\ l_{2\mathrm{s}} = 0.5m.$$

Assuming a maximum of $\pm 25\%$ uncertainty in these parameters, the approximate values of these master and the slave parameters are taken to be

$$\hat{m}_{1\mathrm{m}} = 2.82kg,\ \hat{m}_{2\mathrm{m}} = 2.36kg,\ \hat{l}_{1\mathrm{m}} = 0.62m,\ \hat{l}_{2\mathrm{m}} = 0.56m,$$
$$\hat{m}_{1\mathrm{s}} = 1.16kg,\ \hat{m}_{2\mathrm{s}} = 1.29kg,\ \hat{l}_{1\mathrm{s}} = 0.38m,\ \hat{l}_{2\mathrm{s}} = 0.52m.$$

The controllers $C_{\rm m}$, $C_{\rm s}$, C_1, ..., and C_6 are chosen as in (58), (59) and (60). The controllers and DOB gains and initial conditions are chosen as

$$\begin{array}{ccc} \gamma = 1, & & \\ K_{\rm mv} = 50I & , & K_{\rm sv} = 50I, \\ K_{\rm mp} = 50I & , & K_{\rm sp} = 50I, \\ C_{\rm mf} = I & , & C_{\rm sf} = I, \\ L_{\rm m} = 50I & , & L_{\rm s} = 50I, \\ \hat{f}_{\rm d,m}(0) = 0 & , & \hat{f}_{\rm d,s}(0) = 0, \\ K_{\rm v} = 25I & , & K_{\rm p} = 25I. \end{array}$$

It is to be noted that the master and slave controller and observer gains have been chosen to be equal– this choice is not necessary but is one that results in identical closed-loop master and slave dynamics (63) and (64) when $\Delta d_{\rm m} = 0$ and $\Delta d_{\rm s} = 0$.

Different values for initial joint positions of the master and the slave are chosen while assuming that both robots are initially at rest. The initial joint position vectors are taken to be

$$\begin{aligned} q_{0\rm m} &= [30^\circ, 45^\circ]^T, \\ q_{0\rm s} &= [0, 22.5^\circ]^T. \end{aligned}$$

In the simulations, $f_{\rm e}^* = [0, 0]^T$ and it is assumed that the human operator moves the master end-effector such that the second joint of the master robot moves from 45° to 81.5° while the position of the first joint of the master robot is fixed. The slave end-effector should follow the position of the master end-effector. It is assumed that an external payload, with a mass equal to 0.5^{kg}, is connected to the end-effector of the slave. Also, it is assumed that a sinusoidal disturbance torque equal to $\tau_{\rm d} = \sin(4\pi t)$ is exerted to the second joint of the slave robot. Sinusoidal disturbances are exerted to the joints of a robot in order to examine the efficiency of fault tolerant control schemes.

Figures 14 and 15 show the position tracking responses of the teleoperation system in presence and absence of the NDOBs. Because of the sinusoidal disturbance acting on the second joint of the slave robot, the slave robot end-effector payload, the friction forces and the dynamic uncertainties present in the master and the slave model, the control law without using DOBs fails to achieve good position tracking. As it can be observed from Figures 14 and 15, perfect position tracking has been achieved under the DOB-based control scheme while there are offsets

in the position tracking error under the conventional control scheme. Figure 16 shows the force tracking responses of the teleoperation system in presence and absence of the NDOBs. Figures 17 and 18 show the disturbance tracking of the DOB at the master and the slave sides. As it can be observed from these figures, the disturbances are not constant at the slave side. However, the estimated disturbances tend to follow the actual disturbances with a bounded tracking error.

Future Research Directions

Despite the success of NDOBs in numerous applications, there is a need to expand theoretical studies in this field. There are numerous future research directions that have been highlighted in [11]. The following directions may also be considered in expanding the DOB framework.

- *Extending the NDOB framework to hybrid dynamical control systems:* Hybrid dynamical control systems are a class of control systems that possess both continuous and discrete dynamics [70], [71]. Power systems and mechanical systems subject to impulsive contacts are a few examples that can be modeled as hybrid dynamical systems that are subject to numerous disturbances. The disturbance observer literature is also rich in the context of discrete-time dynamical systems (see [72] and the references therein). However, to the best knowledge of the authors, there has not been any studies regarding the applicability of DOBs to the hybrid settings.
- *Generalizing the NDOB framework from dynamical systems with Euclidean state-spaces to systems with curved state-spaces:* The NDOB framework has thus far been studied in the context of dynamical control systems with Euclidean state-spaces. However, there are many dynamical control systems such as underwater and ground vehicles subject to disturbances whose state-space are not Euclidean [73]. The NDOB framework can be extended to accompany global controllers that are designed for this class of systems.
- *Using NDOBs in underactuated mechanical systems:* Underactuation is a pervasive phenomenon in robotic locomotory systems such as legged robots. Theses systems are subject to various disturbances as they locomote in their ambient environment. Therefore, NDOBs seem to be suitable candidates for disturbance attenuation in these applications. Relaxing the matching condition is an important challenge that arises in the context of underactuated robotics. Early progress has been made to address this challenge in [24].
- *Input observability analysis for NDOBs:* the important analysis of input observability and its geometric interpretation has been largely ignored by the NDOB community. One important reason might be that developing a nonlinear counterpart of matrix pencil decompositions that are used for input observability analysis in LTI systems in [74], is a difficult task.

The input observability analysis is a research direction that NDOB community needs to investigate further.

Concluding Remarks

This article discussed a class of unknown input observers called the nonlinear disturbance observers than can be effectively used in control of robotic and teleoperation systems. Numerous commercial applications of DOBs motivate further theoretical investigation of this class of observers. In this article, several inherent properties of the NDOB proposed in [21] that were not discussed in the previous NDOB literature such as semi/quasi-passivity were shown. Exploiting the inherent properties of EL systems, it was shown that NDOBs can be employed along with passivity-based and computed-torque control schemes without the need to modify these well-established controllers. Applications of NDOBs in the 4-channel teleoperation architecture, which guarantees transparency in the absence of disturbances, were investigated in this article.

References

[1] A. Radke and Z. Gao, "A survey of state and disturbance observers for practitioners," in *Proc. American Control Conference*, 2006, pp. 5183–5188.

[2] K. Ohishi, K. Ohnishi, and K. Miyachi, "Torque-speed regulation of dc motor based on load torque estimation," in *Proc. Int. Conf. IEEJ IPEC*, 1983, pp. 1209–1216.

[3] X. Chen, J. Yang, S. Li, and Q. Li, "Disturbance observer based multi-variable control of ball mill grinding circuits," *J. Process Contr.*, vol. 19, no. 7, pp. 1205–1213, 2009.

[4] J. Yang, S. Li, X. Chen, and Q. Li, "Disturbance rejection of dead-time processes using disturbance observer and model predictive control," *Chem. Eng. Res. Des.*, vol. 89, no. 2, pp. 125–135, 2011.

[5] K. Ohnishi, M. Shibata, and T. Murakami, "Motion control for advanced mechatronics," *IEEE/ASME Trans. Mechatron.*, vol. 1, no. 1, pp. 56–67, Mar. 1996.

[6] Y. Oh and W. K. Chung, "Disturbance-observer-based motion control of redundant manipulators using inertially decoupled dynamics," *IEEE/ASME Trans. Mechatron.*, vol. 4, no. 2, pp. 133–146, 1999.

[7] P. K. Sinha and A. N. Pechev, "Model reference adaptive control of a maglev system with stable maximum descent criterion," *Automatica*, vol. 35, no. 8, pp. 1457–1465, 1999.

[8] P. Zhang and S. X. Ding, "Disturbance decoupling in fault detection of linear periodic systems," *Automatica*, vol. 43, no. 8, pp. 1410–1417, 2007.

[9] B. A. Guvenc, L. Guvenc, and S. Karaman, "Robust mimo disturbance observer analysis and design with application to active car steering," *Int. J. Robust Nonlinear Control*, vol. 20,

pp. 873–891, 2010.

[10] S. Li, J. Yang, W.-h. Chen, and X. Chen, *Disturbance observer-based control: methods and applications*. CRC press, 2014.

[11] W.-H. Chen, J. Yang, L. Guo, and S. Li, "Disturbance observer-based control and related methods: An overview," *IEEE Trans. Ind. Electron.*, 2015, to appear, DOI: 10.1109/TIE.2015.2478397.

[12] K. Ohnishi, "A new servo method in mechatronics," *Trans. Japan Society of Electrical Engineering*, vol. 107-D, pp. 83–86, 1987.

[13] T. Murakami, F. M. Yu, and K. Ohnishi, "Torque sensorless control in multidegree-of-freedom manipulator," *IEEE Trans. Ind. Electron.*, vol. 40, no. 2, pp. 259–265, Apr. 1993.

[14] C. S. Liu and H. Peng, "Disturbance observer based tracking control," *ASME Trans. Dyn. Syst. Meas. Control*, vol. 122, no. 2, pp. 332–335, Jun. 2000.

[15] Q.-C. Zhong and J. E. Normey-Rico, "Control of integral processes with dead-time. part 1: Disturbance observer-based 2dof control scheme," *IEE Proceedings-Control Theory and Applications*, vol. 149, no. 4, pp. 285–290, 2002.

[16] K. Natori, T. Tsuji, K. Ohnishi, A. Hace, and K. Jezernik, "Time-delay compensation by communication disturbance observer for bilateral teleoperation under time-varying delay," *IEEE Trans. Ind. Electron.*, vol. 57, no. 3, pp. 1050–1062, Mar. 2010.

[17] E. Sariyildiz and K. Ohnishi, "Stability and robustness of disturbance-observer-based motion control systems," *IEEE Trans. Ind. Electron.*, vol. 62, no. 1, pp. 414–422, 2015.

[18] ——, "A guide to design disturbance observer," *J. Dyn. Syst. Meas. Control*, vol. 136, no. 2, 2014.

[19] K.-S. Kim, K.-H. Rew, and S. Kim, "Disturbance observer for estimating higher order disturbances in time series expansion," *IEEE Trans. Automat. Contr.*, vol. 55, no. 8, pp. 1905–1911, 2010.

[20] X. Chen, S. Komada, and T. Fukuda, "Design of a nonlinear disturbance observer," *IEEE Trans. Ind. Electron.*, vol. 47, no. 2, pp. 429–437, 2000.

[21] W.-H. Chen, "Disturbance observer based control for nonlinear systems," *IEEE/ASME Trans. Mechatron.*, vol. 9, no. 4, pp. 706–710, 2004.

[22] X. Chen, C.-Y. Su, and T. Fukuda, "A nonlinear disturbance observer for multivariable systems and its application to magnetic bearing systems," *IEEE Trans. Contr. Syst. Technol.*, vol. 12, no. 4, pp. 569–577, 2004.

[23] J. Back and H. Shim, "Adding robustness to nominal output-feedback controllers for uncertain nonlinear systems: A nonlinear version of disturbance observer," *Automatica*, vol. 44, no. 10, pp. 2528–2537, 2008.

[24] J. Yang, S. Li, and W.-H. Chen, "Nonlinear disturbance observer-based control for multi-

input multi-output nonlinear systems subject to mismatching condition," *Int. J. Contr.*, vol. 85, no. 8, pp. 1071–1082, 2012.

[25] H. Shim and N. H. Jo, "An almost necessary and sufficient condition for robust stability of closed-loop systems with disturbance observer," *Automatica*, vol. 45, no. 1, pp. 296–299, 2009.

[26] J. Back and H. Shim, "An inner-loop controller guaranteeing robust transient performance for uncertain mimo nonlinear systems," *IEEE Trans. Automat. Contr.*, vol. 54, no. 7, pp. 1601–1607, 2009.

[27] S. Lichiardopol, N. van de Wouw, D. Kostic, and H. Nijmeijer, "Trajectory tracking control for a tele-operation system setup with disturbance estimation and compensation," in *Proc. IEEE Conf. Decision and Control*, 2010, pp. 1142–1147.

[28] A. Nikoobin and R. Haghighi, "Lyapunov-based nonlinear disturbance observer for serial n-link robot manipulators," *J. Intell. Robot. Syst.*, vol. 55, no. 2-3, pp. 135–153, Jul. 2009.

[29] A. Mohammadi, M. Tavakoli, H. J. Marquez, and F. Hashemzadeh, "Nonlinear disturbance observer design for robotic manipulators," *Control Eng. Pract.*, vol. 21, no. 3, pp. 253–267, 2013.

[30] R. Hao, J. Wang, J. Zhao, and S. Wang, "Observer-based robust control of 6-dof parallel electrical manipulator with fast friction estimation," *IEEE Trans. Autom. Sci. Eng.*, 2015, to appear. DOI: 10.1109/TASE.2015.2427743.

[31] M. Kim and D. Lee, "Toward transparent virtual coupling for haptic interaction during contact tasks," in *Proc. World Haptics Conference*, 2013, pp. 163–168.

[32] T. Floquet, J.-P. Barbot, W. Perruquetti, and M. Djemai, "On the robust fault detection via a sliding mode disturbance observer," *Int. J. Contr.*, vol. 77, no. 7, pp. 622–629, 2004.

[33] X.-G. Yan and C. Edwards, "Nonlinear robust fault reconstruction and estimation using a sliding mode observer," *Automatica*, vol. 43, no. 9, pp. 1605–1614, 2007.

[34] C. E. Hall and Y. B. Shtessel, "Sliding mode disturbance observer-based control for a reusable launch vehicle," *Journal of guidance, control, and dynamics*, vol. 29, no. 6, pp. 1315–1328, 2006.

[35] L. Besnard, Y. B. Shtessel, and B. Landrum, "Quadrotor vehicle control via sliding mode controller driven by sliding mode disturbance observer," *Journal of the Franklin Institute*, vol. 349, no. 2, pp. 658–684, 2012.

[36] T. E. Massey and Y. B. Shtessel, "Continuous traditional and high-order sliding modes for satellite formation control," *Journal of Guidance, Control, and Dynamics*, vol. 28, no. 4, pp. 826–831, 2005.

[37] A. A. Godbole, J. P. Kolhe, and S. E. Talole, "Performance analysis of generalized extended state observer in tackling sinusoidal disturbances," *Control Systems Technology, IEEE Transactions on*, vol. 21, no. 6, pp. 2212–2223, 2013.

[38] S. Li, J. Yang, W.-H. Chen, and X. Chen, "Generalized extended state observer based control for systems with mismatched uncertainties," *Industrial Electronics, IEEE Transactions on*, vol. 59, no. 12, pp. 4792–4802, 2012.

[39] W. H. Chen, D. J. Ballance, P. J. Gawthrop, and J. O'Reilly, "A nonlinear disturbance observer for robotic manipulators," *IEEE Trans. Ind. Electron.*, vol. 47, no. 4, pp. 932–938, Aug. 2000.

[40] A. Mohammadi, H. J. Marquez, and M. Tavakoli, "Disturbance observer based trajectory following control of nonlinear robotic manipulators," in *Proc. Canadian Congress of Applied Mechanics*, Vancouver, BC, Jun. 2011.

[41] J. Huang, S. Ri, L. Liu, Y. Wang, J. Kim, and G. Pak, "Nonlinear disturbance observer-based dynamic surface control of mobile wheeled inverted pendulum," *IEEE Trans. Cont. Syst. Technol.*, 2015, to appear. DOI: 10.1109/TCST.2015.2404897.

[42] T.-S. Lee, "Lagrangian modeling and passivity-based control of three-phase ac/dc voltage-source converters," *IEEE Trans. Ind. Electron.*, vol. 51, no. 4, pp. 892–902, 2004.

[43] A. Tofighi and M. Kalantar, "Power management of pv/battery hybrid power source via passivity-based control," *Renewable Energy*, vol. 36, no. 9, pp. 2440–2450, 2011.

[44] J. M. Scherpen, D. Jeltsema, and J. B. Klaassens, "Lagrangian modeling of switching electrical networks," *Systems & Control Letters*, vol. 48, no. 5, pp. 365–374, 2003.

[45] M. W. Spong, S. Hutchinson, and M. Vidyasagar, *Robot Modeling and Control*. New York: Wiley, 2005.

[46] H. Amini, S. Rezaei, A. A. Sarhan, J. Akbari, and N. Mardi, "Transparency improvement by external force estimation in a time-delayed nonlinear bilateral teleoperation system," *J. Dyn. Syst. Meas. Control*, vol. 137, no. 5, p. 051013, 2015.

[47] A. Mohammadi, M. Tavakoli, and H. J. Marquez, "Control of nonlinear bilateral teleoperation systems subject to disturbances," in *IEEE 50th Conference on Decision and Control*, 2011, pp. 1765–1770.

[48] N. Iiyama, K. Natori, and K. Ohnishi, "Bilateral teleoperation under time-varying communication time delay considering contact with environment," *Electronics and Communications in Japan*, vol. 92, no. 7, pp. 38–46, 2009.

[49] A. Mohammadi, M. Tavakoli, and H. J. Marquez, "Disturbance observer based control of nonlinear haptic teleoperation systems," *IET Control Theory Appl.*, vol. 5, no. 17, pp. 2063–2074, 2011.

[50] ——, "Control of nonlinear teleoperation systems subject to disturbances and variable time delays," in *Proc. IEEE/RSJ Int. Conf. Intell. Robot. Syst.*, 2012, pp. 3017–3022.

[51] T. B. Sheridan, "Telerobotics," *Automatica*, vol. 25, no. 4, pp. 487–507, Jul. 1989.

[52] D. A. Lawrence, "Stability and transparency in bilateral teleoperation," *IEEE Trans. Robot. Autom.*, vol. 9, pp. 624–637, Oct. 1993.

[53] M. Tavakoli, A. Aziminejad, R. Patel, and M. Moallem, "High-fidelity bilateral teleoperation systems and the effect of multimodal haptics," *IEEE Trans. Syst., Man Cybern. B, bern.*, vol. 37, no. 6, pp. 1512–1528, Dec. 2007.

[54] P. Hokayem and M. W. Spong, "Bilateral teleoperation: An historical survey," *Automatica*, vol. 42, pp. 2035–2057, 2006.

[55] E. Sariyildiz, "Advanced robust control via disturbance observer: Implementations in the motion control framework," Ph.D. dissertation, Keio University, 2014.

[56] W.-H. Chen and L. Guo, "Analysis of disturbance observer based control for nonlinear systems under disturbances with bounded variation," in *Proc. Int. Conf. Contr.*, 2004.

[57] H. K. Khalil, *Nonlinear Systems*. Upper Saddle River, NJ: Prentice Hall, 3rd edn, 2002.

[58] A. Abdessameud, I. G. Polushin, and A. Tayebi, "Synchronization of Lagrangian systems with irregular communication delays," *IEEE Trans. Automat. Contr.*, vol. 59, no. 1, pp. 187–193, 2014.

[59] A. Mohammadi, M. Tavakoli, and A. Jazayeri, "PHANSIM: A Simulink toolkit for the SensAble haptic devices," in *Proc. Canadian Congress of Applied Mechanics*, Vancouver, BC, Jun. 2011, pp. 787–790.

[60] S. Katsura, Y. Matsumoto, and K. Ohnishi, "Modeling of force sensing and validation of disturbance observer for force control," in *Proc. IEEE Conf. Ind. Electron. Society*, 2003, pp. 291–296.

[61] K. Natori, T. Tsuji, and K. Ohnishi, "Time delay compensation by communication disturbance observer in bilateral teleoperation systems," in *Proc. IEEE Int. Workshop Adv. Motion Control*, 2006, pp. 218–223.

[62] S. Katsura, Y. Matsumoto, and K. Ohnishi, "Shadow robot for teaching motion," *Robot. Auton. Syst.*, vol. 58, no. 7, pp. 840–846, Jul. 2010.

[63] A. Levant, "Robust exact differentiation via sliding mode technique," *Automatica*, vol. 34, no. 3, pp. 379–384, Mar. 1998.

[64] J. J. Craig, *Introduction to Robotics: Mechanics and Control*. Upper Saddle River, NJ: Pearson Prentice Hall, 2005.

[65] W. H. Zhu and S. E. Salcudean, "Stability guaranteed teleoperation: An adaptive motion/force control approach," *IEEE Trans. Autom. Control*, vol. 45, no. 11, pp. 1951–1969, Nov. 2000.

[66] K. Kosuge, Y. Fujisawa, and T. Fukuda, "Control of mechanical system with man-machine interaction," in *Proc. IEEE/RSJ Int. Conf. Intell. Robots Syst.*, 1992, pp. 87–92.

[67] J. E. Speich, L. Shao, and M. Goldfarb, "Modeling the human hand as it interacts with a telemanipulation system," *Mechatronics*, vol. 15, no. 9, pp. 1127–1142, 2005.

[68] B. Armstrong-Hélouvry, P. Dupont, and C. Canudas-de Wit, "A survey of models, analysis

tools and compensation methods for the control of machines with friction," *Automatica*, vol. 30, no. 7, pp. 1083–1138, 1994.

[69] N. Hung, H. Tuan, T. Narikiyo, and P. Apkarian, "Adaptive control for nonlinearly parameterized uncertainties in robot manipulators," *IEEE Trans. Cont. Syst. Technol.*, vol. 16, no. 3, pp. 458–468, 2008.

[70] A. J. Van Der Schaft and J. M. Schumacher, *An introduction to hybrid dynamical systems*. Springer London, 2000, vol. 251.

[71] R. Goebel, R. G. Sanfelice, and A. Teel, "Hybrid dynamical systems," *IEEE Control Systems*, vol. 29, no. 2, pp. 28–93, 2009.

[72] K.-S. Kim and K.-H. Rew, "Reduced order disturbance observer for discrete-time linear systems," *Automatica*, vol. 49, no. 4, pp. 968–975, 2013.

[73] N. A. Chaturvedi, A. K. Sanyal, and N. H. McClamroch, "Rigid-body attitude control," *IEEE Control Systems*, vol. 31, no. 3, pp. 30–51, 2011.

[74] M. Hou and R. J. Patton, "Input observability and input reconstruction," *Automatica*, vol. 34, no. 6, pp. 789–794, 1998.

[75] E. Naerum, J. Cornella, and O. J. Elle, "Contact force estimation for backdrivable robotic manipulators with coupled friction," in *Proc. IEEE Int. Conf. Intell. Robots Syst.*, 2008, pp. 3021–3027.

[76] B. Taati, A. M. Tahmasebi, and K. Hashtrudi-Zaad, "Experimental identification and analysis of the dynamics of a phantom premium 1.5a hatpic device," *Presence*, vol. 17, no. 4, pp. 327–342, Aug. 2008.

[77] T. Soderstrom and P. Stoica, *System Identification*. Prentice Hall International Ltd, 1989.

[78] K. J. Astrom and B. Wittenmark, *Adatpive Control*. Addison Wesley, 1995.

List of Figures

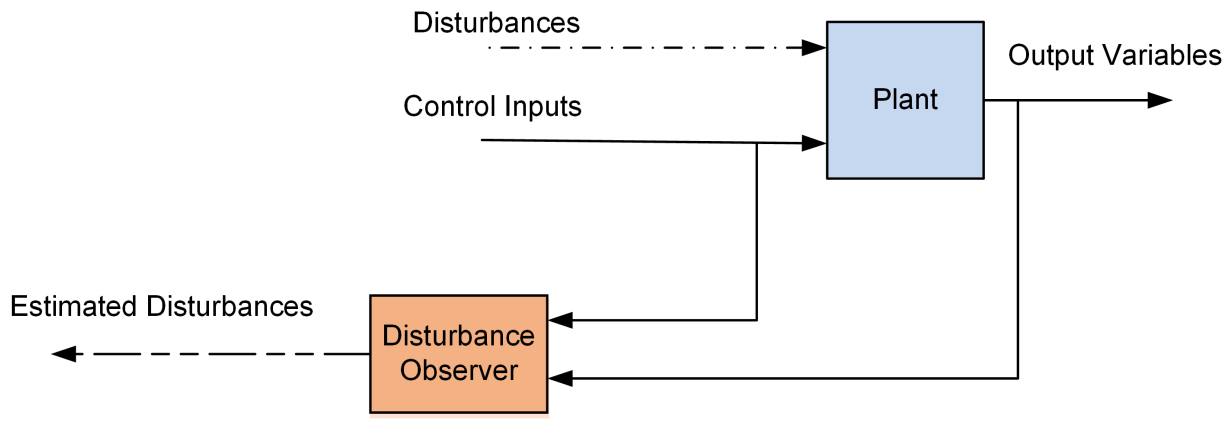

Figure 1: Block diagram of a typical disturbance observer in a control system. The unknown disturbances that are acting on the plant are reconstructed from the measured output variables and the known control inputs applied to the system by the disturbance observer. The output of the disturbance observer, namely, the estimated disturbance, can then be used in feedforward compensation of disturbances or fault detection.

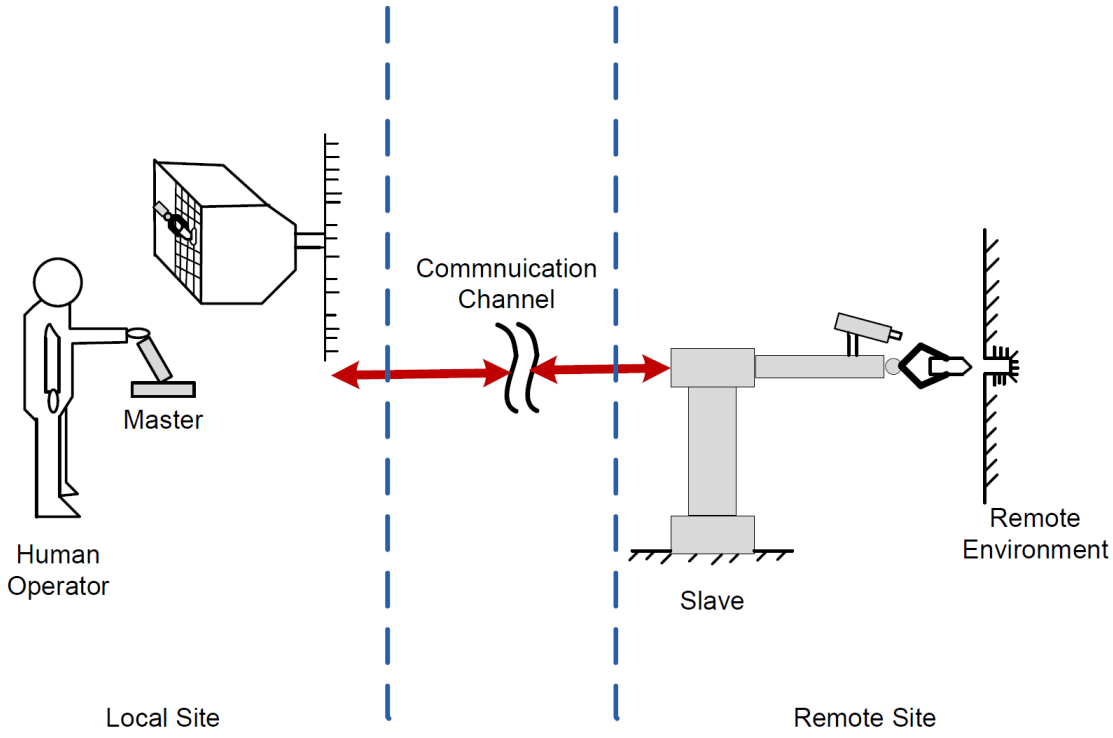

Figure 2: A typical teleoperation system. Teleoperation involves indirect performance of a task in a remote environment and is used to extend a person's sensing and manipulation capability to a remote location. Every teleoperation system consists of a master robot (user interface) and a slave robot, which exchange different types of information such as force, position, and visual and auditory data via a communication channel.

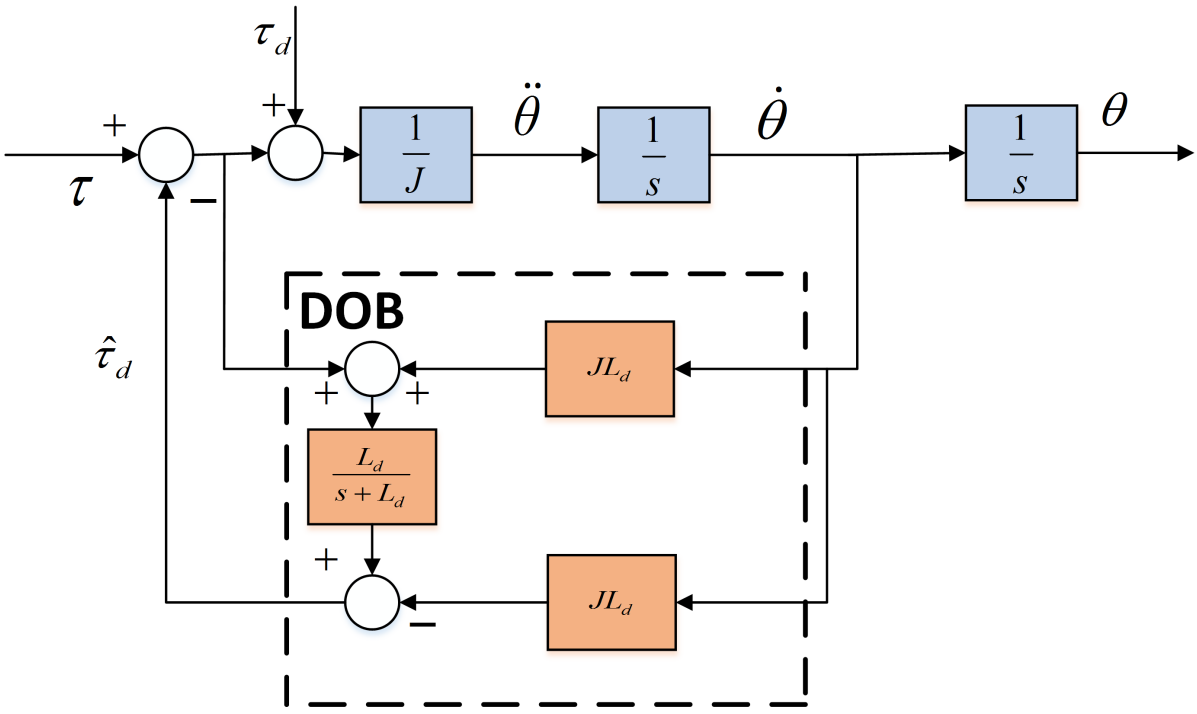

Figure 3: Block diagram of a disturbance observer-based robust motion control system proposed in [2], [12]. The unknown disturbance τ_{d} lumps the effect of external disturbances and plant uncertainties, such as inertia variation and friction. The control input is represented by the torque τ. The parameters J and L_{d} represent mass/inertia and gain of the disturbance observer (DOB), which is a design parameter, respectively.

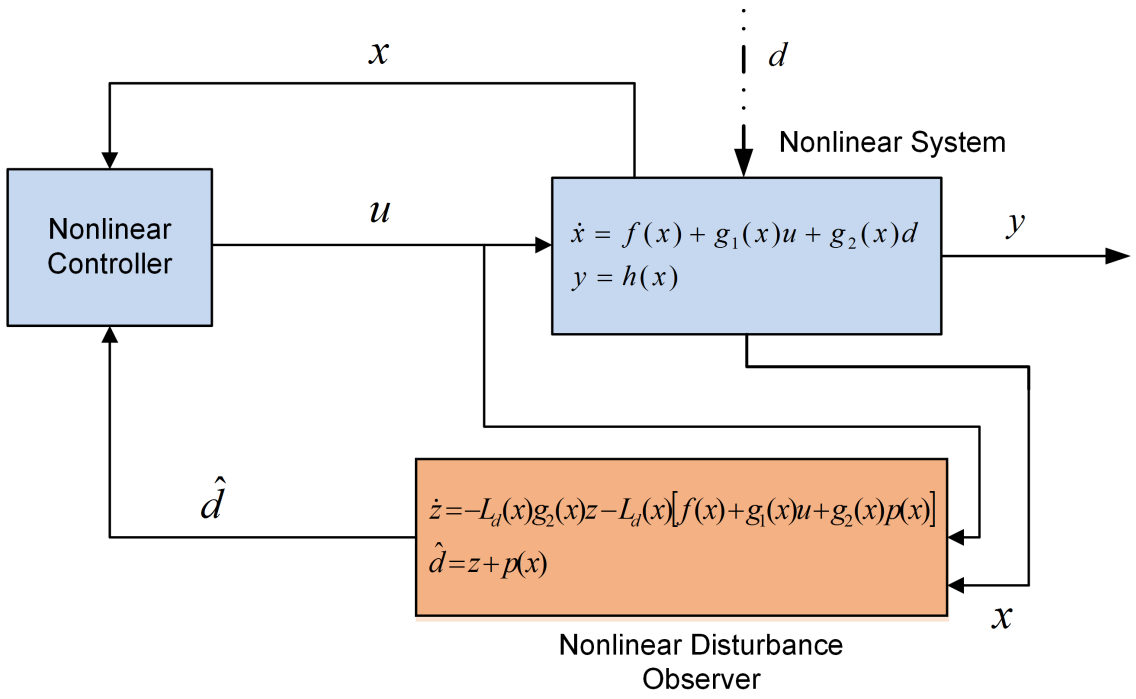

Figure 4: Block diagram of the nonlinear disturbance observer-based robust control system proposed in [21]. The disturbance observer estimates the lumped disturbance vector d from the state and input vectors. The vector $z \in \mathbb{R}^l$ is the internal state vector of the disturbance observer. The matrix $L_{\mathrm{d}}(x)$ is called the DOB gain and satisfies $L_{\mathrm{d}}(x) = \frac{\partial p(x)}{\partial x}$.

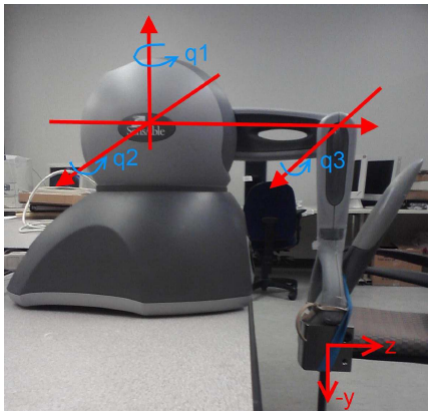

Figure 5: The PHANToM Omni hatpic device and the payload attached to its gimbal. The PHANToM Omni has three actuated revolute joints which provide the user with force feedback information. In addition to the actuated joints, the PHANToM robot has three wrist joints that are passive. The first and the third actuated joints of the PHANToM robot in experiments will be used while the second actuated joint is locked at 0^{deg}. The PHANToM Omni is connected to the computer through an IEEE 1394 port. The PHANToM Omni end-effector position and orientation data are collected at a frequency of 1 kHz. The payload is a metal cube which is attached to the gimbal of the robot.

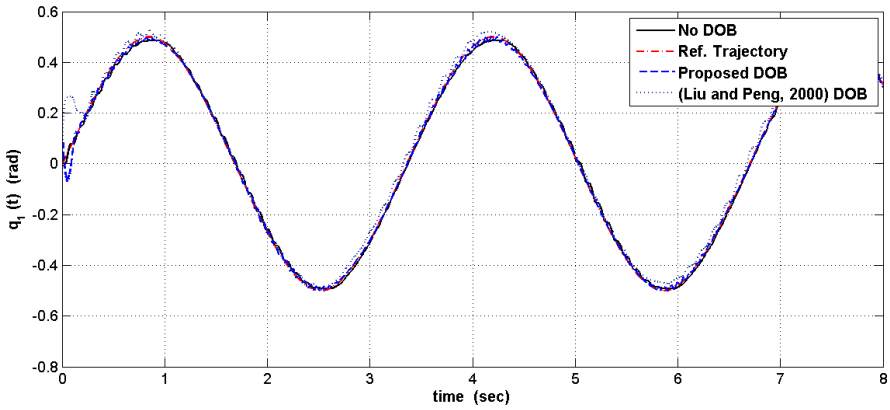

Figure 6: Time profile of position of the first joint of the PHANToM robot. The nonlinear disturbance observer (NDOB), accompanying the computed-torque controller in this experiment, is used to estimate and compensate for the joint frictions and external payload. The payload is a metal cube which is attached to the gimbal of the robot. According to Table 2, the root mean square (RMS) position tracking error of the third joint has been significantly improved using the NDOB structure of [21], [39] with NDOB gain given in [29].

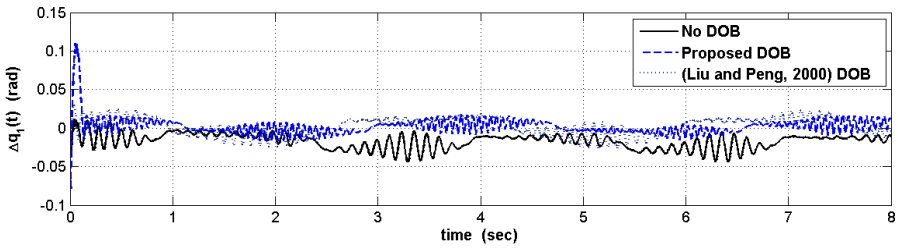

Figure 7: Time profile of position tracking error of the first joint of the PHANToM robot. The nonlinear disturbance observer (NDOB), accompanying the computed-torque controller in this experiment, is used to estimate and compensate for the joint frictions and external payload. The payload is a metal cube which is attached to the gimbal of the robot. According to Table 2, the root mean square (RMS) position tracking error of the third joint has been significantly improved using the NDOB structure of [21], [39] with NDOB gain given in [29].

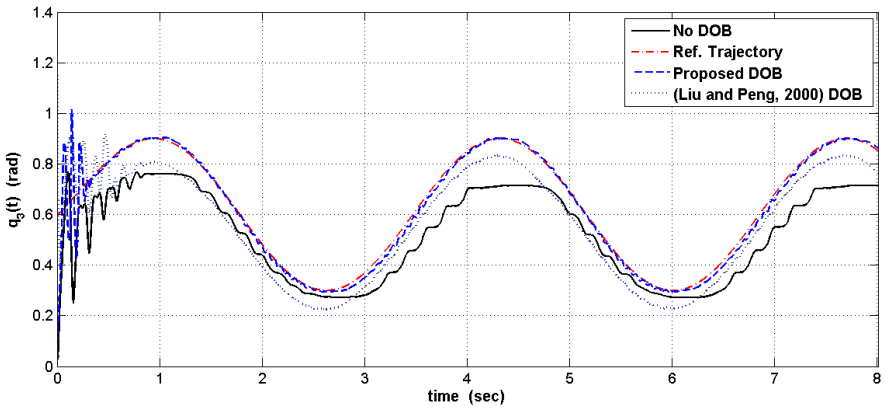

Figure 8: Time profile of position of the third joint of the PHANToM robot. The nonlinear disturbance observer (NDOB), accompanying the computed-torque controller in this experiment, is used to estimate and compensate for the joint frictions and external payload. The payload is a metal cube which is attached to the gimbal of the robot. According to Table 2, the root mean square (RMS) position tracking error of the third joint has been significantly improved using the NDOB structure of [21], [39] with NDOB gain given in [29].

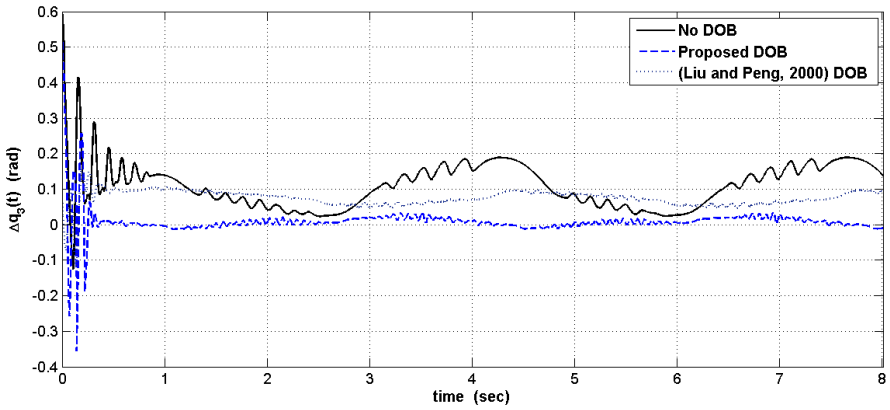

Figure 9: Time profile of position tracking error of the third joint of the PHANToM robot. The nonlinear disturbance observer (NDOB), accompanying the computed-torque controller in this experiment, is used to estimate and compensate for the joint frictions and external payload. The payload is a metal cube which is attached to the gimbal of the robot. According to Table 2, the root mean square (RMS) position tracking error of the third joint has been significantly improved using the NDOB structure of [21], [39] with NDOB gain given in [29].

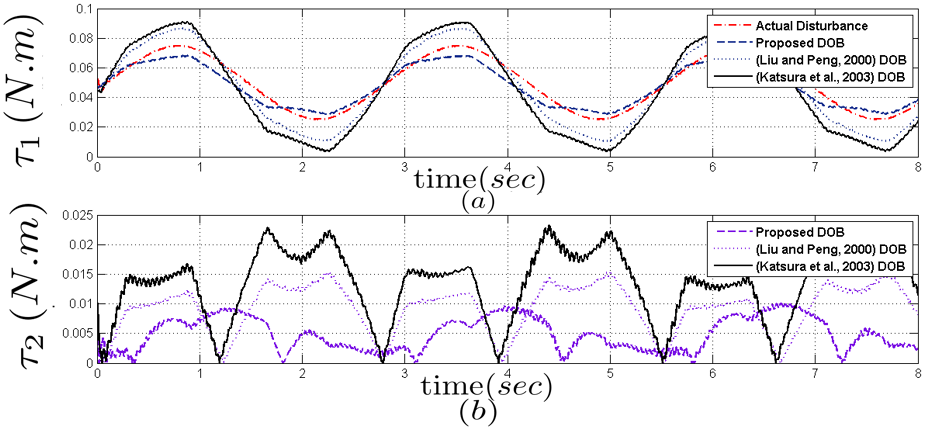

Figure 10: Time profiles of disturbance tracking for the first joint of the PHANToM robot: (a) PHANToM disturbance torque estimation, and (b) PHANToM disturbance torque estimation errors. The nonlinear disturbance observer (NDOB), accompanying the computed-torque controller in this experiment, is used to estimate and compensate for the joint frictions and external payload. The payload is a metal cube which is attached to the gimbal of the robot. According to Table 3, the root mean square (RMS) disturbance tracking error of the third joint has been significantly improved using the NDOB structure of [21], [39] with NDOB gain given in [29].

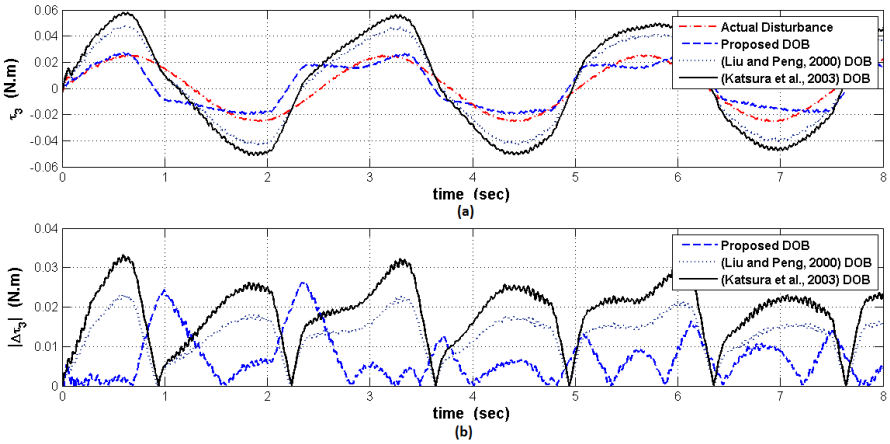

Figure 11: Time profiles of disturbance tracking for the third joint of the PHANToM robot: (a) PHANToM disturbance torque estimation, and (b) PHANToM disturbance torque estimation errors. The nonlinear disturbance observer (NDOB), accompanying the computed-torque controller in this experiment, is used to estimate and compensate for the joint frictions and external payload. The payload is a metal cube which is attached to the gimbal of the robot. According to Table 3, the root mean square (RMS) disturbance tracking error of the third joint has been significantly improved using the NDOB structure of [21], [39] with NDOB gain given in [29].

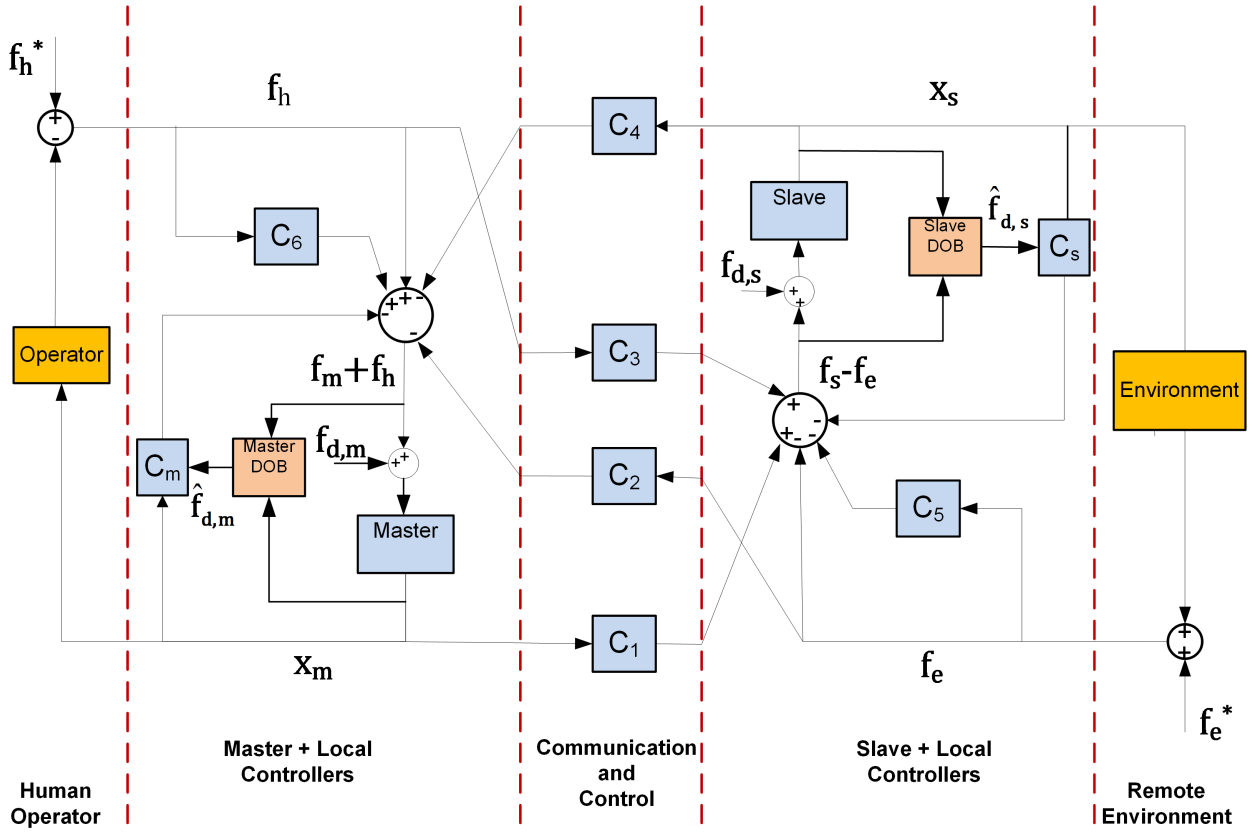

Figure 12: Disturbance observer-based (DOB-based) 4-channel teleoperation control system. Exogenous signals f_{h}^* and f_{e}^* are exerted by the human operator and the remote environment, respectively. The signals x_{m}, x_{s}, f_{h}, f_{e}, f_{m}, f_{s}, $f_{\mathrm{d,m}}$ and $f_{\mathrm{d,s}}$ are as defined in (51)–(52). Position information is exchanged between the master and the slave via the position channels C_1 and C_4. Force information is exchanged through the force channels C_2 and C_3. In addition, C_{m} and C_{s} are local master and slave (position) controllers. Lastly, C_5 and C_6 provide the master and the slave with local force feedback from the human operator and the remote environment, respectively.

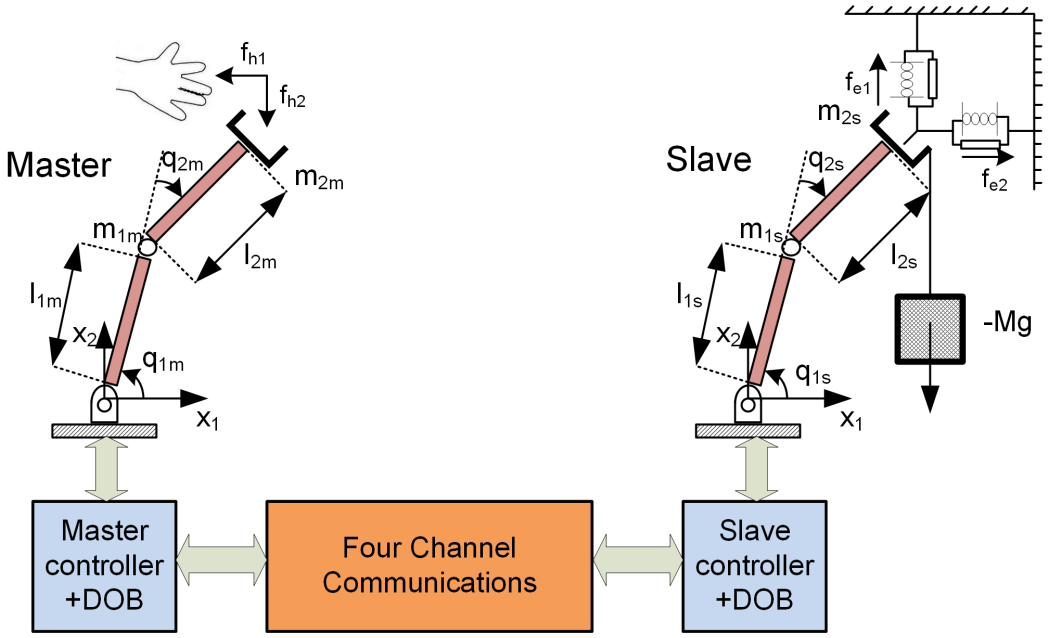

Figure 13: Schematic diagram of the teleoperation system used in simulation. Both the master and the slave robots are considered to be planar two-link manipulators with revolute joints. It is assumed that an external payload, with a mass equal to 0.5^{kg}, is connected to the end-effector of the slave. Also, it is assumed that a sinusoidal disturbance torque equal to $\tau_{\mathrm{d}} = \sin(4\pi t)$ is exerted to the second joint of the slave robot. These external disturbances are exerted to the slave robot in addition to the disturbances due to joint frictions and dynamic uncertainties.

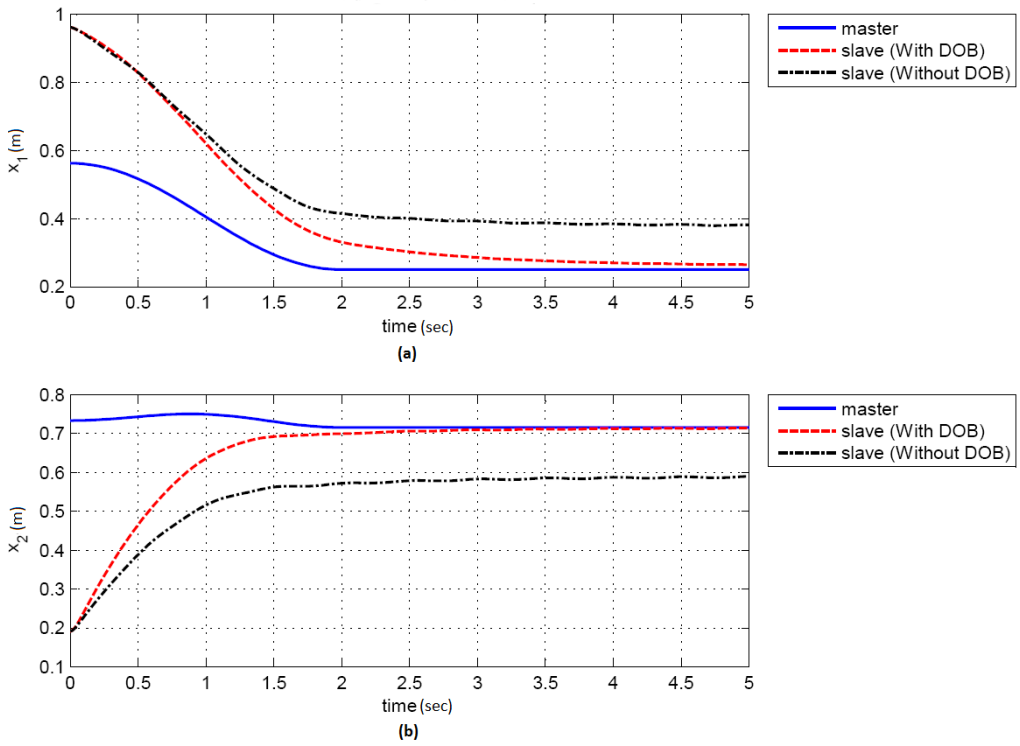

Figure 14: Position tracking of the teleoperation system in the Cartesian space in (a) x_1 coordinate, and (b) x_2 coordinate, with and without disturbance observer (DOB). Both the master and the slave robots are considered to be planar two-link manipulators with revolute joints. It is assumed that an external payload, with a mass equal to 0.5^{kg}, is connected to the end-effector of the slave. Also, it is assumed that a sinusoidal disturbance torque equal to $\tau_{\text{d}} = \sin(4\pi t)$ is exerted to the second joint of the slave robot. Position tracking errors are smaller when nonlinear disturbance observers (NDOBs) are incorporated in the 4-channel teleoperation architecture.

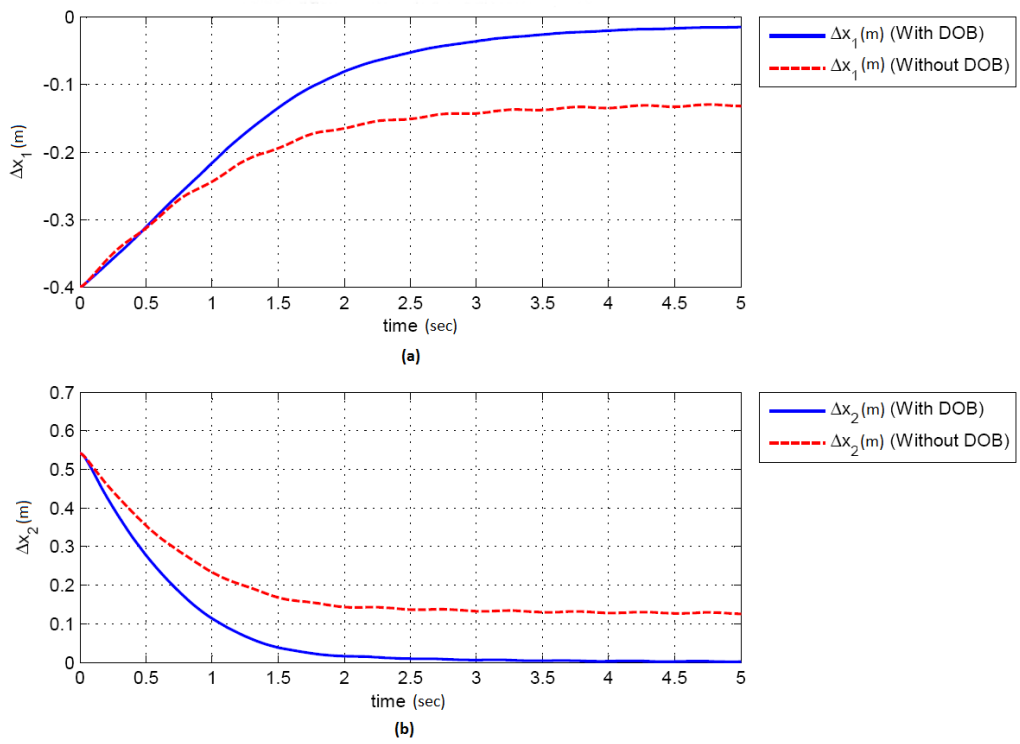

Figure 15: Position tracking error of the teleoperation system in the Cartesian space in (a) x_1 coordinate, and (b) x_2 coordinate, with and without disturbance observer (DOB). Both the master and the slave robots are considered to be planar two-link manipulators with revolute joints. It is assumed that an external payload, with a mass equal to 0.5^{kg}, is connected to the end-effector of the slave. Also, it is assumed that a sinusoidal disturbance torque equal to $\tau_{\text{d}} = \sin(4\pi t)$ is exerted to the second joint of the slave robot. Position tracking errors are smaller when nonlinear disturbance observers (NDOBs) are incorporated in the 4-channel teleoperation architecture.

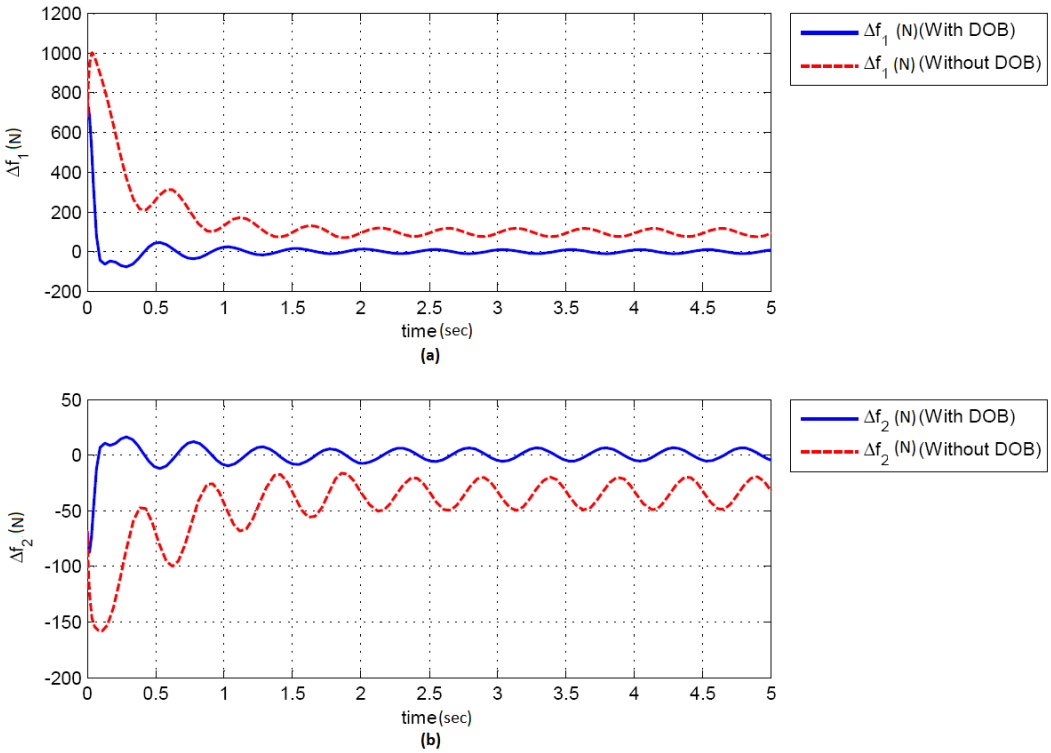

Figure 16: Force tracking of the teleoperation system with and without disturbance observer (DOB). One of the features of the 4-channel architecture is its capability of achieving transparency in the absence of disturbances. As it can be seen from the figure, the force tracking is degraded severely in the presence of disturbances that are not compensated. Force tracking errors are smaller when nonlinear disturbance observers (NDOBs) are incorporated in the 4-channel teleoperation architecture.

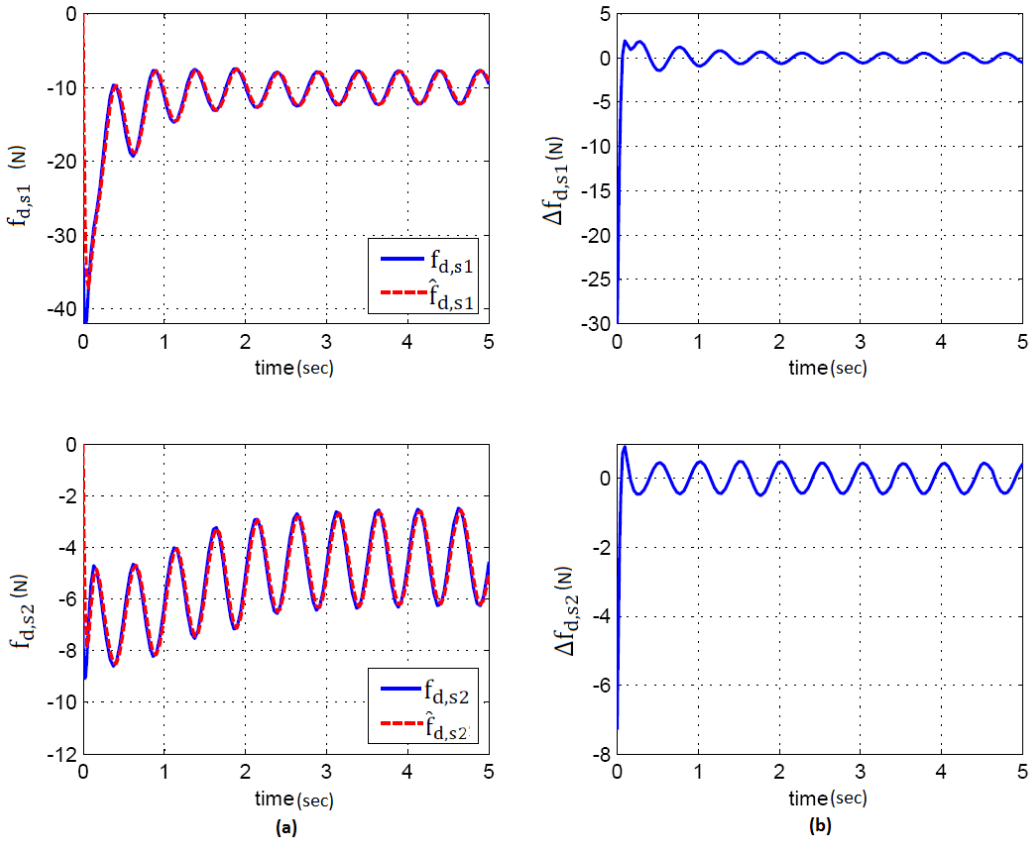

Figure 17: Disturbance tracking at the slave side in (a) x_1 coordinate, and (b) x_2 coordinate. It is assumed that an external payload, with a mass equal to 0.5^{kg}, is connected to the end-effector of the slave. Also, it is assumed that a sinusoidal disturbance torque equal to $\tau_{\text{d}} = \sin(4\pi t)$ is exerted to the second joint of the slave robot. The disturbance tracking errors at the slave side are uniformly ultimately bounded.

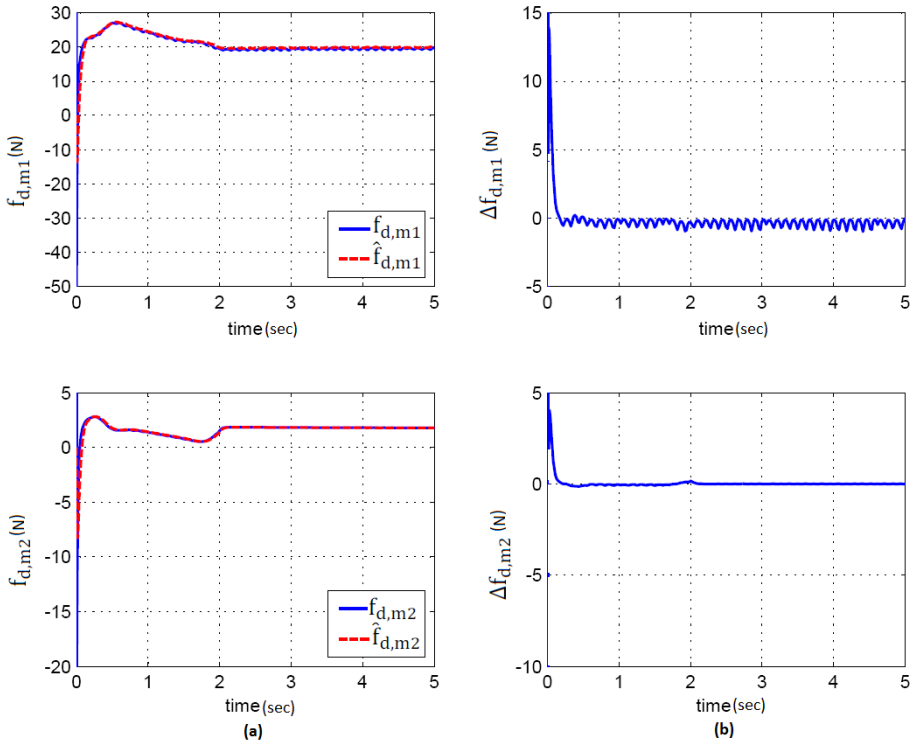

Figure 18: Disturbance tracking at the master side in (a) x_1 coordinate, and (b) x_2 coordinate. It is assumed that an external payload, with a mass equal to 0.5^{kg}, is connected to the end-effector of the slave. Also, it is assumed that a sinusoidal disturbance torque equal to $\tau_{\text{d}} = \sin(4\pi t)$ is exerted to the second joint of the slave robot. The disturbance tracking errors at the master side are uniformly ultimately bounded.

Sidebar 1: Brief Review of Nonlinear Systems

Uniform ultimate boundedness is a useful concept in nonlinear systems literature that can be effectively used for control design. This concept provides a practical notion of stability under certain assumptions.

Definition A solution of the nonlinear system $\dot{x} = f(t, x)$, $x(t) : [t_0, \infty) \to \mathbb{R}^n$ with initial condition $x(t_0) = x_0$ is said to be uniformly ultimately bounded with respect to a set Ω if there exists a constant $T \geq 0$, dependent on x_0 and Ω, such that $x(t) \in \Omega$ for all $t \geq t_0 + T$.

In a closed-loop system, it is desired that the set Ω and the convergence time T depend on control parameters such that with proper design they can be made arbitrarily small. Moreover, if the domain of attraction can be arbitrarily enlarged by tuning control parameters, it is said that the closed-loop system is semi-globally practically stable. The following theorem gives a sufficient condition for having the uniform ultimate boundedness property in terms of existence of a Lyapunov function.

Theorem 1 (Uniform Ultimate Boundedness): Let $\mathcal{B}_r(0)$ be the open ball centered at the origin with radius r and $V : \mathcal{B}_{r_0}(0) \times [0, \infty) \to \mathbb{R}^n$ be a continuously differentiable function such that

$$c_1|x|^2 \leq V(x,t) \leq c_2|x|^2,$$
$$\frac{\partial V}{\partial x} f(x,t) + \frac{\partial V}{\partial t} \leq -c_3|x|^2, \text{ for all } |x| \geq \mu > 0,$$

for all $t \geq 0$ and all $x \in \mathcal{B}_r(0)$. Take $r_0 > 0$ such that $r_0 < r$ and $\mu < r_0$. Then, for every initial state $x(t_0) \in \mathcal{B}_{r_0}(0)$, the trajectories of the system converge with an exponential rate proportional to c_3 to a ball centered at the origin with a radius proportional to $\frac{1}{c_3}$. Moreover, these trajectories enter the ball in a finite time $T > 0$ dependent on μ and $x(t_0)$, and remain within the ball after $t_0 + T$.

The next theorem guarantees the existence of suitable Lyapunov functions when the system is exponentially stable.

Theorem 2 (Converse Lyapunov Theorem): Let $x = 0$ be an equilibrium point for the nonlinear system $\dot{x} = f(t, x)$, where $f : [0, \infty) \times \to \mathbb{R}^n$ is continuously differentiable, $\mathcal{B}_r(0)$ is the open ball centered at the origin with radius r, and the Jacobian matrix $[\frac{\partial f}{\partial x}]$ is bounded on $\mathcal{B}_r(0)$, uniformly in t. Let k, λ, and r_0 be positive constants with $r_0 < r/k$. Let $\mathcal{B}_{r_0}(0)$ be the open ball centered at the origin with radius r_0. If the trajectories of the system satisfy

$$|x(t)| \leq k|x(t_0)|e^{-\lambda(t-t_0)}, \text{ for all } x(t_0) \in \mathcal{B}_{r_0}(0), \text{ and all } t \geq t_0 \geq 0.$$

Then, there exists a function $V : \mathcal{B}_{r_0}(0) \times [0, \infty) \to \mathbb{R}^n$ that satisfies the inequalities

$$\begin{aligned} &c_1|x|^2 \leq V(x,t) \leq c_2|x|^2, \\ &\frac{\partial V}{\partial x} f(x,t) + \frac{\partial V}{\partial t} \leq -c_3|x|^2, \\ &\left|\frac{\partial V}{\partial x}\right| \leq c_4|x|, \end{aligned}$$

for some positive constants c_1, c_2, c_3, and c_4.

One of the fundamental concepts in analyzing the stability of nonlinear systems is that of passivity. Passive systems, such as linear circuits that only contain positive resistors, possess desirable stability properties. Consider the nonlinear control affine system

$$\begin{aligned} \dot{x} &= f(x) + g(x)u, \\ y &= h(x). \end{aligned} \tag{S1}$$

The system (S1) is said to be *passive* if there exists a nonnegative differentiable function, called the storage function, V with $V(0) = 0$ and nonnegative continuous function H with $H(0) = 0$ such that for all admissible inputs and initial conditions $x(0) = x_0$ the following inequality holds:

$$\dot{V}(x,u) \leq y^T u - H(x). \tag{S2}$$

A weaker notion of passivity that is used in this article is that of *quasi-passivity* (or *semi-passivity*) that was first introduced in [S3] (see also [S4]). The system (S1) is said to semi-passive in $\mathcal{D} \subset \mathbb{R}^n$, if there exists a nonnegative function $V : \mathcal{D} \to \mathbb{R}^+$, $\mathcal{D}$ is open, connected and invariant under (S1) such that for all admissible inputs, for all initial conditions in $\mathcal{D}$, and for all time instants t for which the solutions of (S1) exist, the following inequality holds:

$$\dot{V}(x,u) \leq y^T u - H(x), \tag{S3}$$

where the function $H(x)$ is nonnegative outside the ball $\mathcal{B}_r(0) \subset \mathcal{D}$ for some positive constant r. If $\mathcal{D} = \mathbb{R}^n$, the system (S1) is called semi-passive.

One of the properties of semi-passive systems is that these systems behave similar to passive systems for large enough $|x|$. It can be shown that an output feedback of the form $u = \xi(y)$ such that $y^T \xi(y) \leq 0$ makes the solutions of the semi-passive system ultimately bounded (see [S3], [S4] for more details).

References

[S1] H. J. Marquez, *Nonlinear Control Systems*, Hoboken, NJ: John Wiley & Sons, Inc., 2003.

[S2] M. W. Spong, S. Hutchinson, and M. Vidyasagar, *Robot Modeling and Control*, New York: Wiley, 2005.

[S3] I. G. Polushin, "Stability results for quasidissipative systems", in *Proc. 3rd European Control Conf.*, Rome, Italy, 1995.

[S4] I. G. Polushin, D. Hill, and A. L. Fradkov, "Strict quasipassivity and ultimate boundedness for nonlinear control systems", in *Proc. 4th IFAC Symp. Nonlin. Cont. Syst. (NOLCOS)*, Enschede, The Netherlands, 1998, pp. 527–532.

Sidebar 2: PHANToM Omni and its Parameter Identification

The PHANToM Omni® (Geomagic Inc., SC, USA) is a haptic device that can be employed in various applications such as virtual reality and teleoperation. The PHANToM Omni has three actuated revolute joints which provide the user with force feedback information. In addition to the actuated joints, the PHANToM robot has three wrist joints that are passive.

The PHANToM dynamic model can be found in different sources (see, for example, [S5]). Defining $c_i = \cos(q_i)$, $s_i = \sin(q_i)$, $c_{2.i} = \cos(2q_i)$, and $s_{2.i} = \sin(2q_i)$, the inertia matrix of the PHANToM robot, assuming $q_2 = 0$, is given by [S5]:

$$\mathbf{M}(\mathbf{q}) = \begin{bmatrix} \alpha_1 + \alpha_2 c_{2.3} + \alpha_3 s_{2.3} + \alpha_4 c_3 + \alpha_5 s_3 & 0 \\ 0 & \alpha_6 \end{bmatrix}, \tag{S4}$$

and defining

$$\mathbf{V}(\mathbf{q}, \dot{\mathbf{q}}) = [V_1, V_2]^T = \mathbf{C}(\mathbf{q}, \dot{\mathbf{q}})\dot{\mathbf{q}} + \mathbf{G}(\mathbf{q}), \tag{S5}$$

where the vector $\mathbf{V}(\mathbf{q}, \dot{\mathbf{q}})$ is the sum of the Coriolis, centrifugal and gravity forces, it is seen that

$$\begin{aligned} V_1 &= -2\alpha_2 \dot{q}_1 \dot{q}_3 \sin(2q_3) + 2\alpha_3 \dot{q}_1 \dot{q}_3 \cos(2q_3) \\ &\quad + \alpha_4 \dot{q}_1 \dot{q}_3 \cos(q_3) - \alpha_5 \dot{q}_1 \dot{q}_3 \sin(q_3), \\ V_2 &= 2\alpha_2 \dot{q}_1^2 \cos(q_3)\sin(q_3) - \alpha_3 \dot{q}_1^2 \cos(2q_3) - \\ &\quad \frac{1}{2}\alpha_4 \dot{q}_1^2 \cos(q_3) + \frac{1}{2}\alpha_5 \dot{q}_1^2 \sin(q_3) \\ &\quad + \alpha_7 \sin(q_3) + \alpha_8 \cos(q_3). \end{aligned} \tag{S6}$$

The Jacobian of the PHANToM, considering $q_2 = 0$, is [S5]:

$$\mathbf{J}(\mathbf{q}) = \begin{bmatrix} l_1 + l_2 s_3 & 0 \\ 0 & l_1 s_3 \end{bmatrix}, \tag{S7}$$

where $l_1 = l_2 = 135^{mm}$ are the lengths of the first and the second link of the robot. Therefore, the disturbance due to the external payload which is being exerted to the first and the third joints of the robot is:

$$\boldsymbol{\tau}_{payload} = \mathbf{J}^T\mathbf{F} = \mathbf{J}^T \begin{bmatrix} 0 \\ mg \end{bmatrix} = \begin{bmatrix} 0 \\ mgl_1 s_3 \end{bmatrix}. \tag{S8}$$

The PHANToM parameters can be identified in the absence of external payloads using the method proposed in [S7]. This method uses the dynamic equation of the PHANToM in the *linearly parameterized* form (see Property P4 of EL systems)

$$Y(\ddot{q}, \dot{q}, q)\alpha = \tau, \tag{S9}$$

where $Y \in \mathbb{R}^{2\times 8}$ is the regressor matrix and $\alpha = [\alpha_1, \ldots, \alpha_8]^T \in \mathbb{R}^{8\times 1}$ is the vector of robot parameters to be identified. The expression for the PHANToM regressor matrix is [S5]

$$\mathbf{Y}^T = \begin{bmatrix} \ddot{q}_1 & 0 \\ \ddot{q}_1 c_{2.3} - 2\dot{q}_1\dot{q}_3 s_{2.3} & 2\dot{q}_1^2 c_3 s_3 \\ \ddot{q}_1 s_{2.3} + 2\dot{q}_1\dot{q}_3 c_{2.3} & -\dot{q}_1^2 c_{2.3} \\ \ddot{q}_1 s_3 + \dot{q}_1\dot{q}_3 c_3 & -\frac{1}{2}\dot{q}_1^2 c_3 \\ \ddot{q}_1 c_3 - \dot{q}_1\dot{q}_3 s_3 & \frac{1}{2}\dot{q}_1^2 s_3 \\ 0 & \ddot{q}_3 \\ 0 & s_3 \\ 0 & c_3 \end{bmatrix}. \tag{S10}$$

According to the method in [S7] and in order to avoid acceleration measurements, the dynamic model (S9) needs to be passed through a first order stable low-pass filter of the form $\frac{\omega_L}{s+\omega_L}$. In the parameter identification process, the cut-off frequency of the filter is chosen to be to equal to 8 Hz because this frequency is between noise frequencies and robot motion frequencies. After passing through the low-pass filter, the dynamic equation (S9) becomes

$$Y_L(\dot{q}, q)\alpha = \tau_L, \tag{S11}$$

TABLE S1: PHANToM Omni identified parameters: The PHANToM parameters can be identified in the absence of external payloads using the method proposed in [S7]. This method uses the dynamic equation of the PHANToM in the *linearly parameterized* form. In the identification process, the first and the third joints of the PHANToM were under PD (proportional-derivative) control and the second joint was locked at 0^{deg}.

Parameter	Value	Parameter	Value
α_1	$6.11 \times 10^{-3} \pm 0.9 \times 10^{-3}$	α_2	$-2.89 \times 10^{-3} \pm 0.43 \times 10^{-3}$
α_3	$-4.24 \times 10^{-3} \pm 1.01 \times 10^{-3}$	α_4	$3.01 \times 10^{-3} \pm 0.52 \times 10^{-3}$
α_5	$2.05 \times 10^{-3} \pm 0.15 \times 10^{-3}$	α_6	$1.92 \times 10^{-3} \pm 0.23 \times 10^{-3}$
α_7	$1.60 \times 10^{-1} \pm 0.05 \times 10^{-1}$	α_8	$-8.32 \times 10^{-3} \pm 2.78 \times 10^{-3}$

where Y_L is the filtered regressor matrix and τ_L is the filtered torque. A sum of 8 sinusoids, 4 sinusoids for each of the joints 1 and 3, with frequencies ranging from 0.2 Hz to 1 Hz were applied to the PHANToM to identify the 8 unknown parameters. For a persistent excitation of order no less than $2n-2$, the sum of n sinusoids needs to be applied to an unknown plant for identification purposes [S8]. In the identification process, the first and the third joints of the PHANToM were under PD (proportional-derivative) control and the second joint was locked at 0^{deg}. The role of the simple position PD controller employed in the identification is to make the robot joints traverse persistently exciting trajectory profiles. In order to find the parameters of the PHANToM, the recursive least squares algorithm is employed [S6]. Following this procedure, the PHANToM parameters were identified; accordingly, Table S1 gives the PHANToM Omni identified parameters.

References

[S5] E. Naerum, J. Cornella, and O. J. Elle, "Contact force estimation for backdrivable robotic manipulators with coupled friction", in *Proc. IEEE Int. Conf. Intell. Robots Syst.*, Nice, France, pp. 3021-3027.

[S6] K. J. Astrom and B. Wittenmark, *Adatpive Control*, Addison Wesley, 1995.

[S7] B. Taati, A. M. Tahmasebi, and K. Hashtrudi-Zaad, "Experimental identification and analysis of the dynamics of a PHANToM Premium 1.5A hatpic device", *Presence*, vol. 17, no. 4, pp. 327–342, 2008.

[S8] T. Soderstrom and P. Stoica, *System Identification*, Prentice Hall, 1989.

Sidebar 3: Brief Review of Euler-Lagrange Systems

The model of a fully actuated EL system with an N-dimensional configuration space $\mathcal{Q} = \mathbb{R}^N$ is given by

$$\frac{d}{dt}\frac{\partial \mathcal{L}}{\partial \dot{q}} - \frac{\partial \mathcal{L}}{\partial q} = \tau, \tag{S12}$$

where $q \in \mathcal{Q}$ is the vector of generalized coordinates, $\dot{q} \in T_q\mathcal{Q} = \mathbb{R}^N$ is vector of the generalized velocities, and $\tau \in \mathbb{R}^N$ is the vector of control inputs. The Lagrangian function $\mathcal{L}(q, \dot{q}) : T\mathcal{Q} = \mathbb{R}^{2N} \to \mathbb{R}$ is a smooth function and assumed to have the form [S9]

$$\mathcal{L}(q, \dot{q}) = \mathcal{T}(q, \dot{q}) - \mathcal{V}(q), \tag{S13}$$

where $\mathcal{T}(q, \dot{q})$ is the kinetic energy function and $\mathcal{V}(q)$ is the potential function which is assumed to be smooth and bounded from below.

In the case of electrical networks, $\mathcal{T}(q, \dot{q})$ is the sum of the magnetic co-energies of the inductive elements in terms of the currents through the inductors, while $\mathcal{V}(q)$ is given by the sum of the electric field energies of the capacitive elements in terms of the charges on the capacitors (see [S10] for further details). In the case of mechanical systems, $\mathcal{T}(q, \dot{q})$ is the sum of mechanical kinetic energies. We have $\mathcal{T}(q, \dot{q}) = \frac{1}{2}\dot{q}^T M(q)\dot{q}$ where $M(q) \in \mathbb{R}^{N\times N}$ is the generalized inertia matrix and is assumed to be symmetric and positive definite. The reader is referred to [S11] for the general case of Lagrangian systems with non-Euclidean configuration spaces.

Substituting (S13) in (S12) yields

$$M(q)\ddot{q} + N(q, \dot{q}) = \tau + \tau_{\mathrm{d}}, \tag{S14}$$

where,

$$N(q, \dot{q}) = C(q, \dot{q})\dot{q} + G(q), \tag{S15}$$

and $C(q, \dot{q})\dot{q} \in \mathbb{R}^N$ is the vector of Coriolis and centrifugal forces. Also, $G(q) := \frac{\partial \mathcal{V}}{\partial q}$ are the forces generated by potential fields such as the gravitational field.

Following the EL systems literature (see, for example, [S9]), it is assumed that the EL model under study has the following properties:

P1

1) The inertia matrix $M(q)$ satisfies

$$\nu_1 I \leq M(q) \leq \nu_2 I, \tag{S16}$$

where ν_1 and ν_2 are some positive constants and Inequality (S16) holds uniformly with respect to q.

2) The matrix $\dot{M}(q) - 2C(q,\dot{q})$ is skew-symmetric; namely, $z^T\big[\dot{M}(q) - 2C(q,\dot{q})\big]z = 0$ for all $z \in \mathbb{R}^N$.

3) The matrix $C(q,\dot{q})$ is bounded in q and linear in $\dot{q}$; namely,

$$C(q,\dot{q})z = C(q,z)\dot{q}, \tag{S17}$$

$$\big|C(q,\dot{q})\big| \leq k_c|\dot{q}|, \tag{S18}$$

for all $z \in \mathbb{R}^N$ and some positive constant k_c.

4) Let $q_r \in \mathbb{R}^n$ be an arbitrary vector. There exists a linear parameterization for EL models of the form $M(q)\ddot{q}_{\rm r} + C(q,\dot{q})\dot{q}_{\rm r} + G(q) = \Upsilon(q,\dot{q},\dot{q}_{\rm r},\ddot{q}_{\rm r})\theta$, where Υ is a regressor matrix of known functions and θ is a vector containing EL system parameters.

References

[S9] R. Ortega, A. Loría, P. J. Nicklasson, and H. Sira-Ramírez, *Passivity-based Control of Euler-Lagrange Systems*, Springer-Verlag, London, 1998.

[S10] J. MA. Scherpen, D. Jeltsema, and J. B. Klaassens, "Lagrangian modeling of switching electrical networks", *Systems & Control Letters*, vol. 48, no. 5, pp. 365–374, 2003.

[S11] F. Bullo and A. D. Lewis, *Geometric control of mechanical systems: modeling, analysis, and design for simple mechanical control systems*, Springer Science & Business Media, 2004.

Author Information

Alireza Mohammadi (alireza.mohammadi@mail.utoronto.ca) is currently a Ph.D. candidate in the Department of Electrical and Computer Engineering at the University of Toronto, Canada. He received the M.Sc. degree in Electrical and Computer Engineering from the University of Alberta, Canada in 2009. His research interests include robotic locomotion, medical and rehabilitation robotics, and nonlinear control theory.

Horacio J. Marquez (hmarquez@ualberta.ca) received the B. Sc. degree from the Instituto Tecnologico de Buenos Aires (Argentina), and the M.Sc.E and Ph.D. degrees in electrical engineering from the University of New Brunswick, Fredericton, Canada, in 1987, 1990 and 1993, respectively.

From 1993 to 1996 he held visiting appointments at the Royal Roads Military College, and the University of Victoria, Victoria, British Columbia. In 1996 he joined the Department of Electrical and Computer Engineering, University of Alberta, as an Assistant Professor, becoming Associate Professor in 2000, and Professor in 2003. From 2000 to 2004 he was Associate Chair of Graduate Studies, and from 2004 to 2014 he was Chair of Electrical and Computer Engineering at the University of Alberta. His current research interest include nonlinear filtering and control, robust control, sampled-data systems, and control of cyber-physical systems. He is the Author of Nonlinear Control Systems: Analysis and Design (Wiley, 2003).

Dr. Marquez is a Licensed Professional Engineer (PEng) and a Fellow of the Canadian Academy of Engineering (CAE), Fellow of the Engineering Institute of Canada (EIC), Fellow of the Institution of Engineering and Technology (EIT), and a Senior Member of the IEEE.

Mahdi Tavakoli (mahdi.tavakoli@ualberta.ca) is an Associate Professor in the Department of Electrical and Computer Engineering, University of Alberta, Canada. He received his BSc and MSc degrees in Electrical Engineering from Ferdowsi University and K.N. Toosi University, Iran, in 1996 and 1999, respectively. He received his PhD degree in Electrical and Computer Engineering from the University of Western Ontario, Canada, in 2005. In 2006, he was a post-doctoral researcher at Canadian Surgical Technologies and Advanced Robotics (CSTAR), Canada. In 2007-2008, he was an NSERC Post-Doctoral Fellow at Harvard University, USA. Dr. Tavakolis research interests broadly involve the areas of robotics and systems control. Specifically, his research focuses on haptics and teleoperation control, medical robotics, and image-guided surgery. Dr. Tavakoli is the lead author of Haptics for Teleoperated Surgical Robotic Systems (World Scientific, 2008).